NAVAL POSTGRADUATE SCHOOL

MONTEREY, CALIFORNIA

THESIS

ANALYSIS OF THE FAILURE OF A VACUUM SPIN-PIT DRIVE TURBINE SPINDLE SHAFT

by

Jason M. Pettitt

September 2005

Thesis Advisor: R.P.Shreeve
Second Reader: T.R.McNelley

Approved for public release; distribution is unlimited

THIS PAGE INTENTIONALLY LEFT BLANK

REPORT DOCUMENTATION PAGE	*Form Approved OMB No. 0704-0188*

1. AGENCY USE ONLY ***(Leave blank)***	**2. REPORT DATE** September 2005	**3. REPORT TYPE AND DATES COVERED** Master's Thesis

4. TITLE AND SUBTITLE: Analysis of the Failure of a Vacuum Spin-Pit Drive Turbine Spindle Shaft	**5. FUNDING NUMBERS**
6. AUTHOR(S) Jason M. Pettitt	
7. PERFORMING ORGANIZATION NAME(S) AND ADDRESS(ES) Naval Postgraduate School Monterey, CA 93943-5000	**8. PERFORMING ORGANIZATION REPORT NUMBER**
9. SPONSORING /MONITORING AGENCY NAME(S) AND ADDRESS(ES) N/A	**10. SPONSORING/MONITORING AGENCY REPORT NUMBER**

11. SUPPLEMENTARY NOTES The views expressed in this thesis are those of the author and do not reflect the official policy or position of the Department of Defense or the U.S. Government.

12a. DISTRIBUTION / AVAILABILITY STATEMENT Approved for public release; distribution is unlimited	**12b. DISTRIBUTION CODE**

13. ABSTRACT (maximum 200 words)

The Naval Postgraduate School's Rotor Spin Research Facility experienced a failure in the Spring of 2005 in which the rotor dropped from the drive turbine and caused extensive damage. A failure analysis of the drive turbine spindle shaft was conducted in order to determine the cause of failure: whether due to a material or design flaw. Also, a dynamic analysis was conducted in order to determine the natural modes present in the system and the associated frequencies that could have contributed to the failure of the shaft. It was concluded that the failure was due to low cycle fatigue, a possible stress concentration was identified, and a torsional mode was found near the speed at which failure occurred.

14. SUBJECT TERMS Austenitization, Beachmarks, Cementite, Coalescence, Ductile, Fatigue, Martensite, Microvoid Formation, Mode(s), Mode Shapes, Natural Frequencies, Rockwell Hardness, Rotor Dynamics, Scanning Electron Microscope(SEM), Striations, Tempering, Torsion	**15. NUMBER OF PAGES** 65
	16. PRICE CODE

17. SECURITY CLASSIFICATION OF REPORT	**18. SECURITY CLASSIFICATION OF THIS PAGE**	**19. SECURITY CLASSIFICATION OF ABSTRACT**	**20. LIMITATION OF ABSTRACT**
Unclassified	Unclassified	Unclassified	UL

NSN 7540-01-280-5500 Standard Form 298 (Rev. 2-89)
Prescribed by ANSI Std. 239-18

THIS PAGE INTENTIONALLY LEFT BLANK

Approved for public release; distribution is unlimited

ANALYSIS OF THE FAILURE OF A VACUUM SPIN-PIT DRIVE TURBINE SPINDLE SHAFT

Jason M. Pettitt
Ensign, United States Navy
B.S., Ocean Engineering, United States Naval Academy, 2004

Submitted in partial fulfillment of the
requirements for the degree of

MASTER OF SCIENCE IN MECHANICAL ENGINEERING

from the

NAVAL POSTGRADUATE SCHOOL
September 2005

Author: Jason M. Pettitt

Approved by: Raymond P. Shreeve
Thesis Advisor

Terry R. McNelley
Second Reader/Co-Advisor

Anthony J. Healey
Chairman, Department of Mechanical and Astronautical Engineering

THIS PAGE INTENTIONALLY LEFT BLANK

ABSTRACT

The Naval Postgraduate School's Rotor Spin Research Facility experienced a failure in the spring of 2005 in which the rotor dropped from the drive turbine and caused extensive damage. A failure analysis of the drive turbine spindle shaft was conducted in order to determine the cause of failure: whether due to a material or design flaw. Also, a dynamic analysis was conducted in order to determine the natural modes present in the system and the associated frequencies that could have contributed to the failure of the shaft. It was concluded that the failure was due to low cycle fatigue, a possible stress concentration, and a torsional mode was found near the speed at which failure occurred.

THIS PAGE INTENTIONALLY LEFT BLANK

TABLE OF CONTENTS

THIS PAGE INTENTIONALLY LEFT BLANK

LIST OF FIGURES

THIS PAGE INTENTIONALLY LEFT BLANK

LIST OF TABLES

THIS PAGE INTENTIONALLY LEFT BLANK

ACKNOWLEDGMENTS

First I would like to acknowledge my thesis advisor, Professor Raymond P. Shreeve. He was an invaluable mentor whose vast knowledge aided me in my work. Also, I would like to thank Doug Seivwright who was willing to discuss, listen and help in anyway possible at any given time regardless of how busy he might have been. Lastly, I would like to thank Professor Terry R. McNelley for providing additional insight and teaching me the fundamentals of material failure and analysis.

THIS PAGE INTENTIONALLY LEFT BLANK

I. INTRODUCTION

A. BACKGROUND

The Rotor Spin Research Facility is located in the Turbopropulsion Laboratory at the Naval Postgraduate School. The facility utilizes an 8-inch Barbour-Stockwell air driven turbine to spin test rotors in order to evaluate techniques proposed for testing and improving the high cycle fatigue behavior of rotor blades.

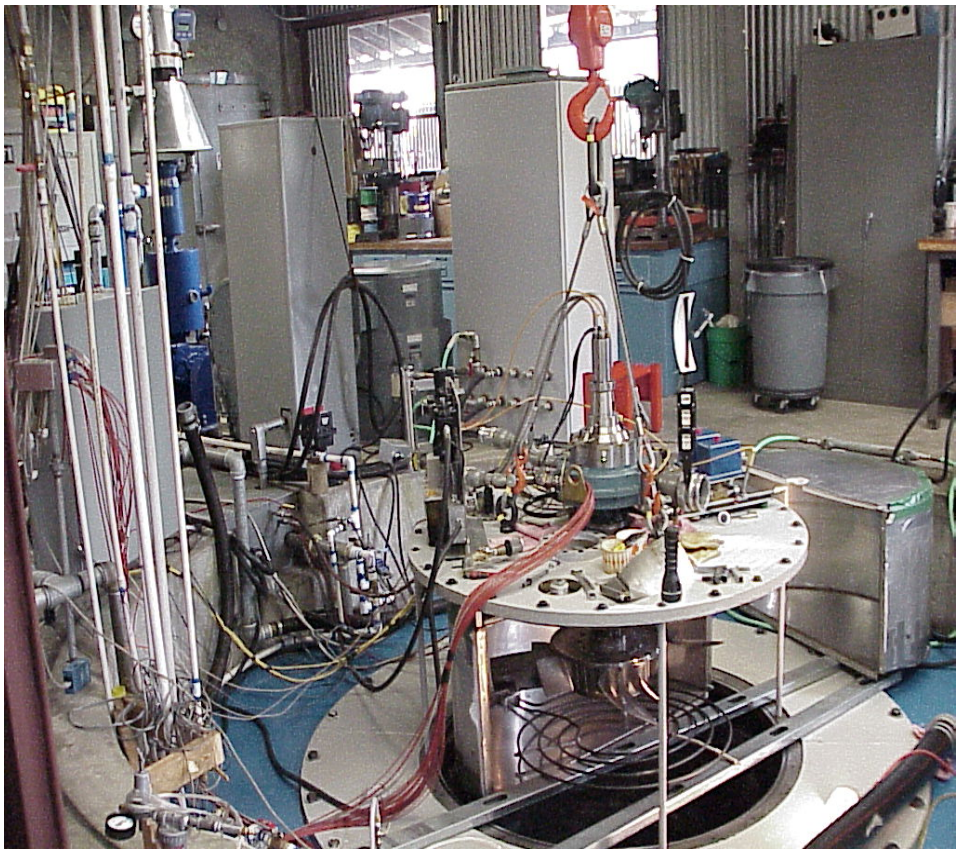

Figure 1. Rotor Spin Research Facility

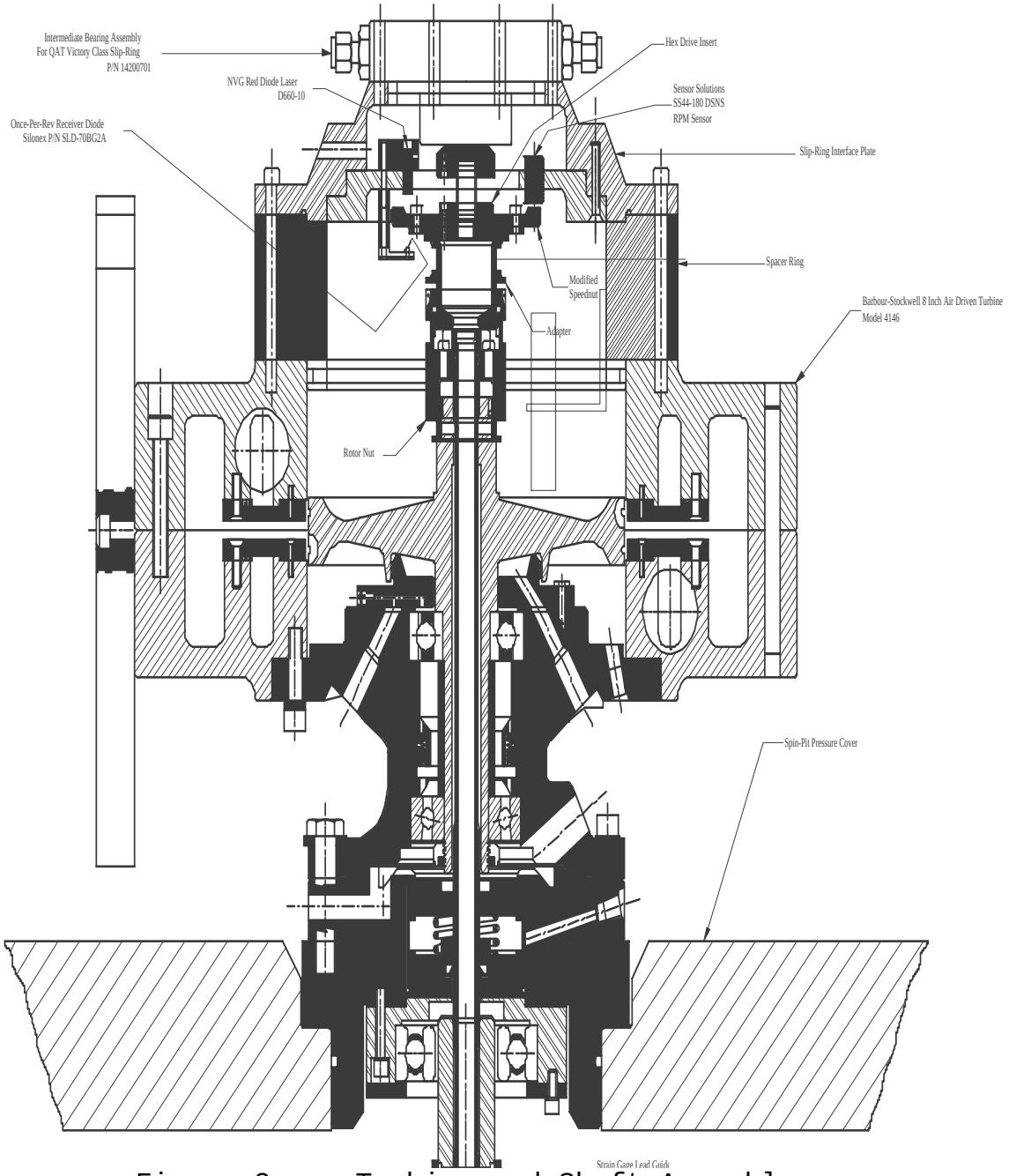

Figure 2. Turbine and Shaft Assembly

Figure 2 shows the turbine assembly and its complexity. At the time of the failure, the turbine was connected to the rotor test article by a hollow spindle shaft. The shaft was 14.775” in length, and had an outer diameter of 0.625” and an inner diameter of 0.400”. The shaft was suspended on a button resting on a horizontal surface in the air turbine and was secured by a threaded nut.

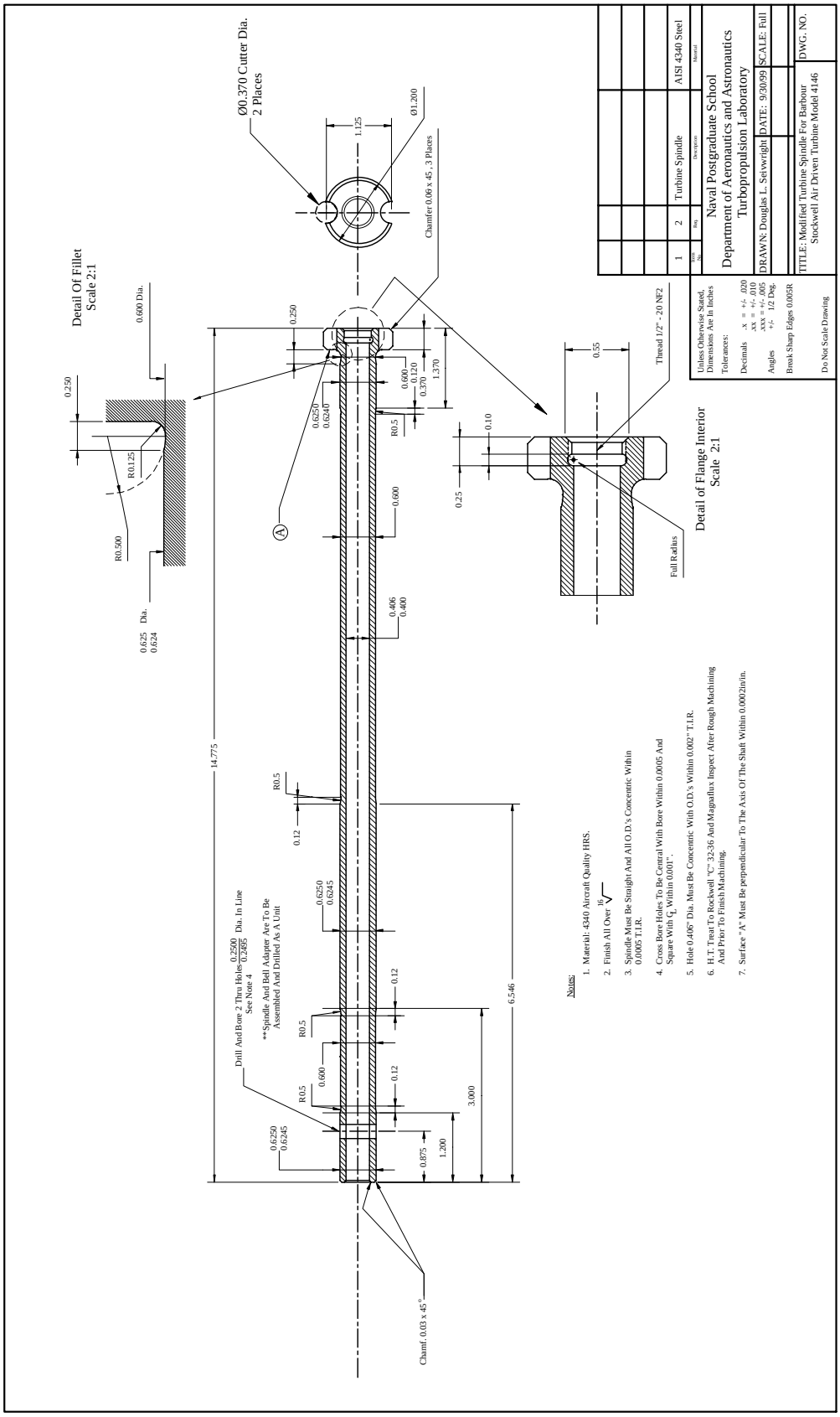

Figure 3. Design Drawing of the Spindle Drive Shaft

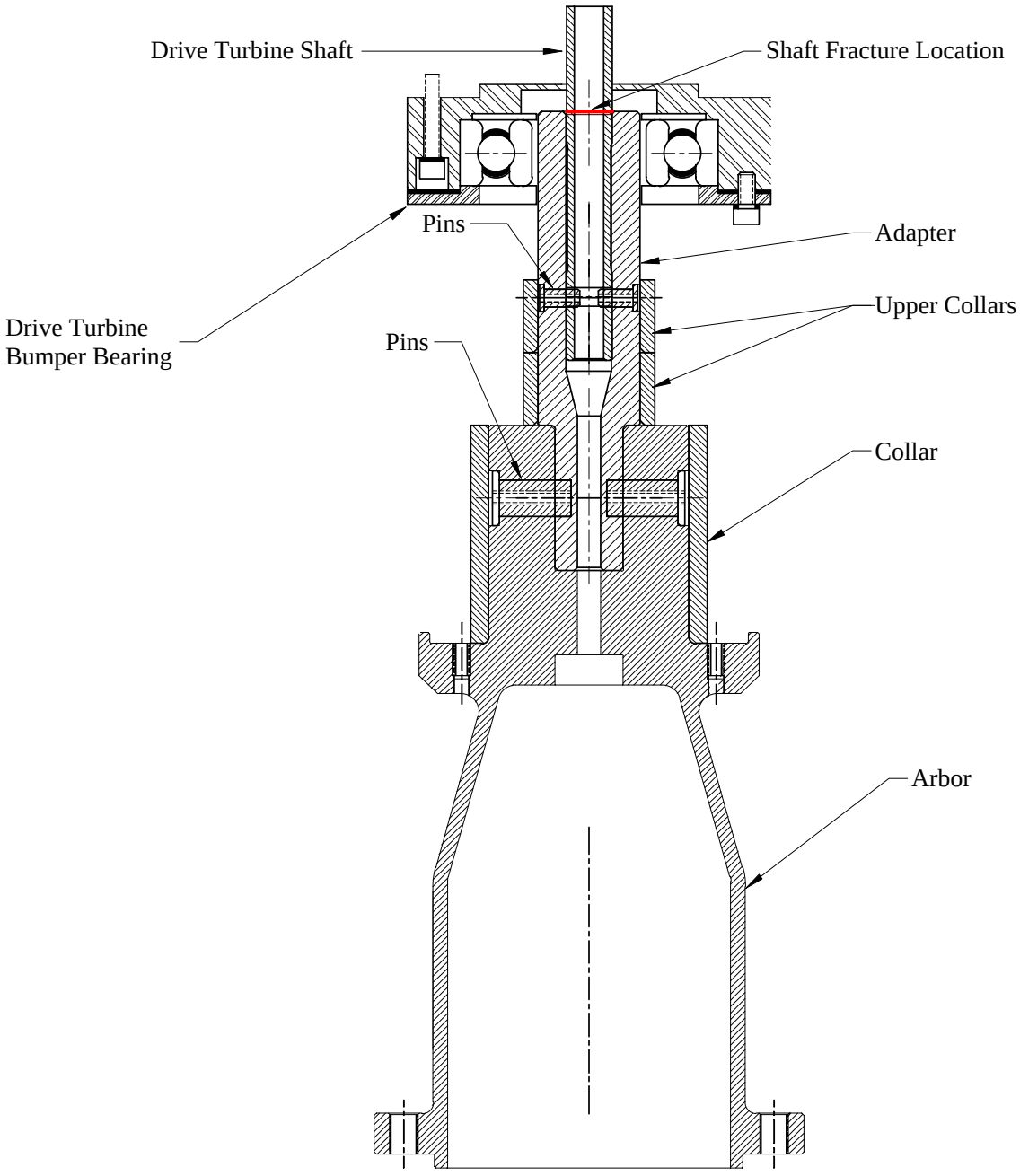

Figure 4. Arbor and Suspension System Assembly for AE3007 Rotor

Figure 3 shows the design drawing for the spindle drive shaft, and Figure 4 shows how the shaft was connected to the adapter, collar and arbor. The test rotor was attached to the flange at the bottom of the arbor. The

spindle shaft was connected to the rotor adapter through a pinned connection with two threaded screws that transmitted torque.

B. FAILURE

On 14 March 2005, the Rotor Spin Research Facility began testing a revised oil nozzle configuration for blade excitation. The AE3007 (Configuration 2), shown in Figure 5, was the rotor that was installed.

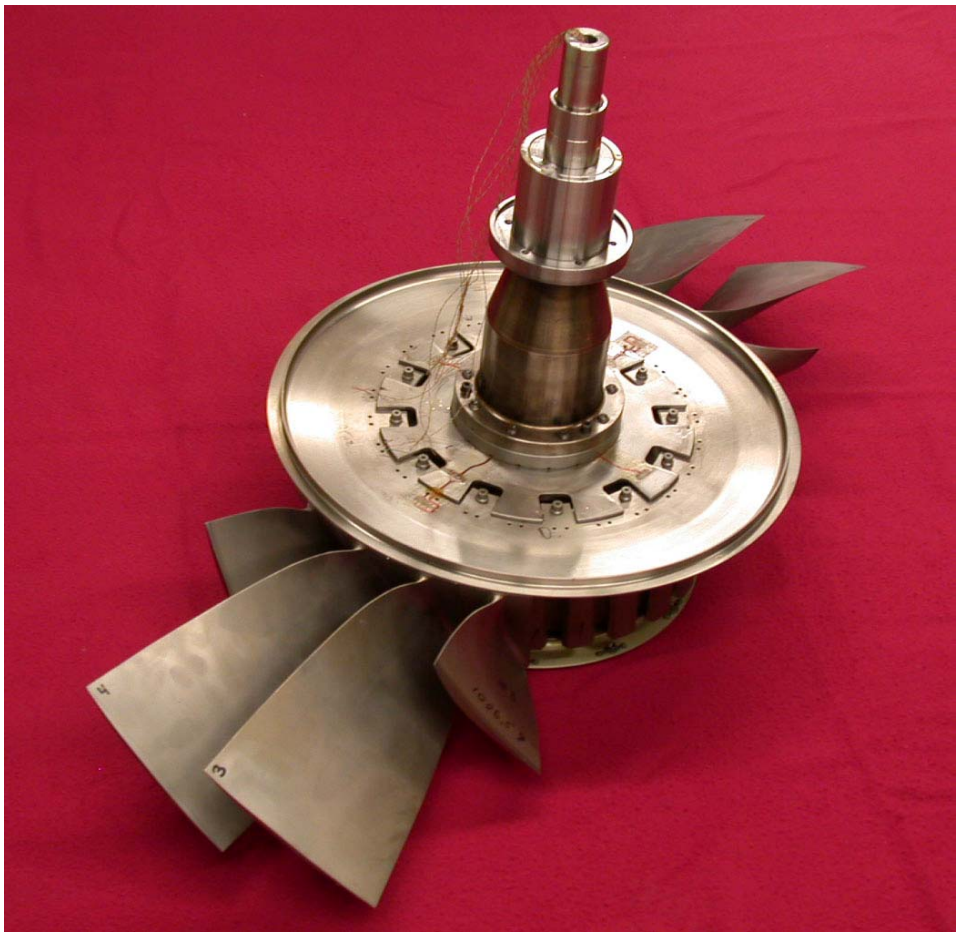

Figure 5. AE3007 (Configuration 2) Fan Rotor

Normal operation for a new build required the system to be spun up quickly to 1000 RPM, and then standard checks would be performed on the instrumentation. Once all checks were completed, the speed would be increased to a target of

7600 RPM. However, during this initial run, while checks were being made of the instrumentation, the RPM drifted up to around 1600 RPM. Once the operator realized the upward drift, the speed was immediately increased to 2000 RPM. Once all checks were completed, the RPM was then steadily increased towards the target speed. After about 15-18 minutes of operation, and at about 2500 RPM, the spindle shaft failed, dropping the rotor into the spin pit. There was extensive damage done within the pit. All instrumentation and the oil-excitation system were destroyed. However, the pit itself, and the stainless steel liner which collected the injected oil, were intact.

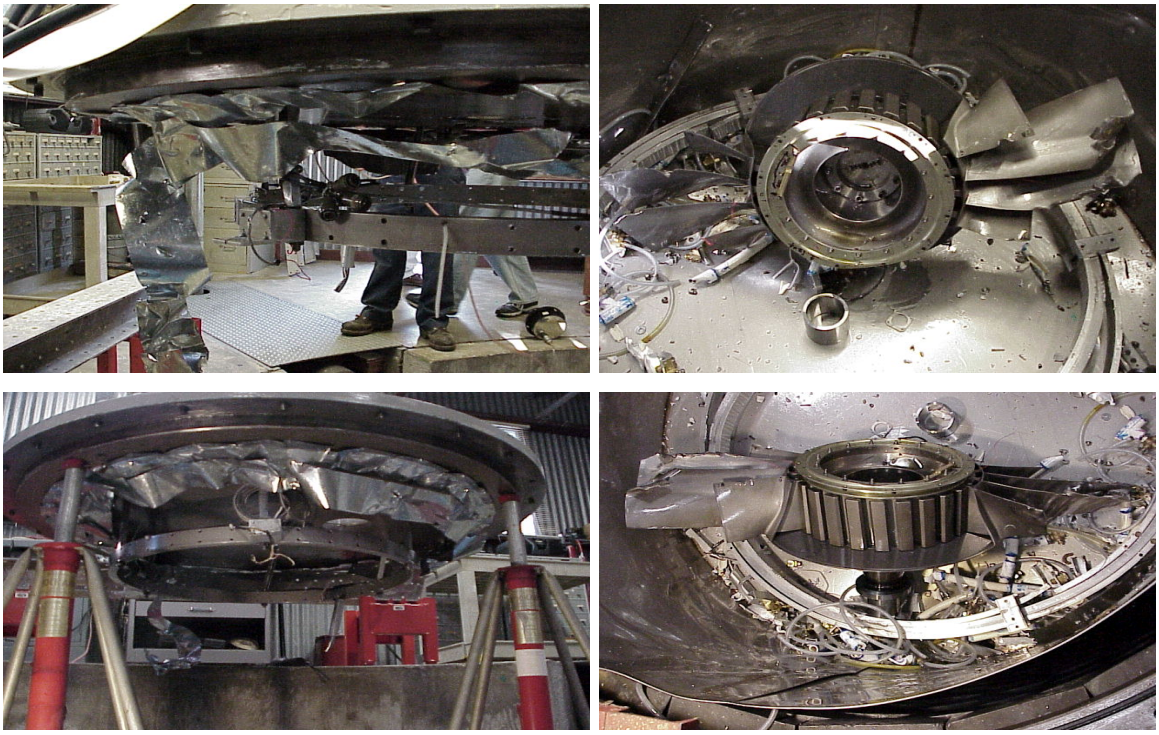

Figure 6. Images of Failure Aftermath

The purpose of the present study was to investigate the possible cause(s) of the shaft failure in order to prevent future failures from occurring.

C. SHAFT USAGE HISTORY

After failure occurred, the Rotor Spin Research Facility's logbooks were reviewed. It was found that the shaft in question had been in use for a number of years and had been used with five different test rotors. When in operation, the system was run anywhere from several minutes to several hours. Table 1 shows the history of the shaft usage with each different test article. The column for estimated Partial LCF cycles was not included in this document and is outside of the scope of this research.

Table 1. Drive Spindle Shaft Usage

Rotor	Brief Description	# Runs	Max Operating RPM of Rotor	RPM Range For Full LCF Cycles	Estimated Full LCF Cycles	Estimated Partial LCF Cycles	*Nominal Runout In Specified Ranges	**Max Runout Noted In Specified Ranges
M-1 Rotor	Diameter = 36 Inches Weight = 225 lbs.	86	9000	0-2000	90	None Noted	System Proved Unstable	80 mils
11 Inch Transonic Rotor	Diameter = 11Inches Weight = 5 lbs.	41	27,000	0-5,000	11	See Figure 5	Unknown	Unknown
				0-10,000	6		34 mils	41 mils / 6,000 RPM
				0-15,000	6		27 mils	33.5 mils / 12,500 RPM
				0-20,000	7		30.0 mils	40 mils / 17,500 RPM
				0-25,000	15		31.35 MILS	35 mils / 25,000 RPM
				0-30,000	3		35 mils	Unknown
11 Inch Titanium Rotor	Diameter = 11 Inches Weight = 10 lbs.	21	27,000	0-5,000	3	See Figure 6	23.75 mils	29.15 mils / 5000 RPM
				0-10,000	2		24.85 mils	29.15 mils / 10,000 RPM
				0-15,000	0		22.3 mils	24.75 mils / 13,000 RPM
				0-20,000	15		20 mils	30.65 mils / 17,500 RPM
				0-25,000	0		21.75 mils	25 mils / 22,700 RPM
				0-30,000	1		18.4 mils	23.55 mils / 27,000 RPM
XTE-66	Diameter = 22 Inches, Weight =170 lbs.	53	12,000	0-5,000	2	See Figure 7	12.5 mils	16.2 mils / 3250 RPM
				0-10,000	78		8.5 mils	12.25 mils/ 6000 RPM
				0-15,000	1		5.35 mils	8.15 mils / 10,000 RPM
AE3007 (Configuration 1)	Diameter = 38 inches Weight = 210 lbs.	60	10,000	0-5,000	3	See Figure 8	Initial Tests = 12.5 mils, Latter Tests = 22.5 mils	33.0 mils / 2000 RPM
				0-10,000	58		Initial tests = 17.2 mils, Latter Tests, 9.9 mils	17.6 mils / 8200 RPM
AE3007 (Configuration 2)	Diameter = 38 inches Weight = 210 lbs.	9	10,000	0-5,000	0	See Figure 9	19 mils	24.75mils /
				0-10,000	9		14.25 mils /3,000 RPM	16.90mils / 7,800 RPM

II. MATERIAL BACKGROUND

A. SPINDLE FORMING

The spindle shaft was constructed from AISI 4340 steel. This is a hypoeutectoid (0.4% carbon) Fe-C alloy steel with roughly 3% weight additions of chromium, molybdenum, and nickel. The spindle was specified to be a seamless, hollowed bored shaft with Rockwell C hardness between 32 and 36.

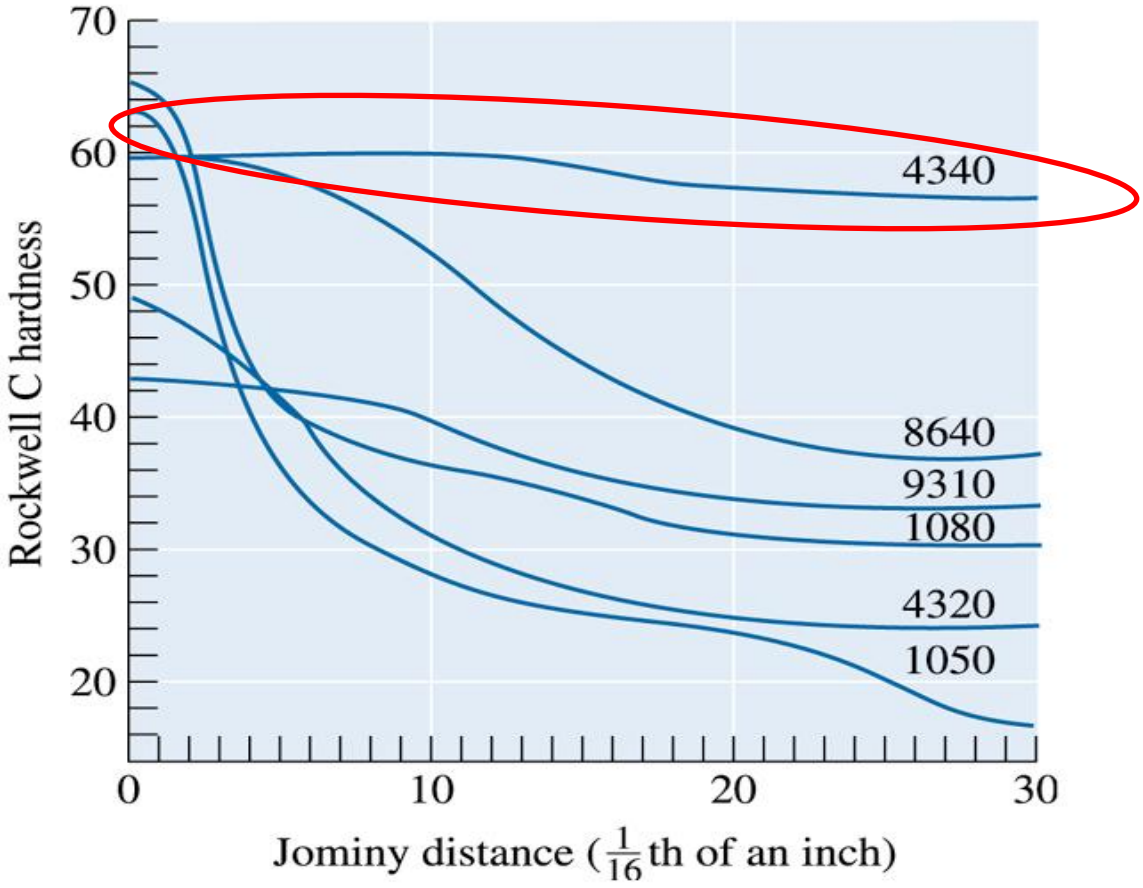

Figure 7. Hardness Plot for Various Steels (After Ref. 1)

As shown in Figure 7, 4340 steel has exceptional hardenability and is commonly used in the construction of

pistons, gears, etc. Depending upon the heat treatment of the steel, the hardness can range anywhere from 17 to 60+ on the Rockwell Hardness C scale.

B. HEAT TREATMENT

There are many heat treatments currently used when preparing 4340 steel. Fortunately, because the spindle shaft was specified to have 32-36 HRC the potential treatments narrowed to a small group. Based upon information taken from Aerospace Materials® data sheets, 4340 steel with a HRC of 32-36 is most commonly heat treated by first austenitizing at 800-830^{o}C, followed by an oil quench, and concluding with extended tempering at 540-595^{o}C.

The tempering chart for 4340 steel, shown in Figure 8, shows the considerable loss in strength/hardness and the increase in ductility that accompanies such a heat treatment. Although there is a considerable loss in strength, it is important that the shaft not be too hard and therefore low in toughness. The heat treatment of the shaft also increases its ductility. All of these factors help prevent against brittle fracture, which is never a desirable mode of fracture. With a more ductile shaft, signs of failure and deformation should be present before a failure occurs. Finally, this heat treatment with a subsequent high tempering will also significantly increase the grain size of the steel.

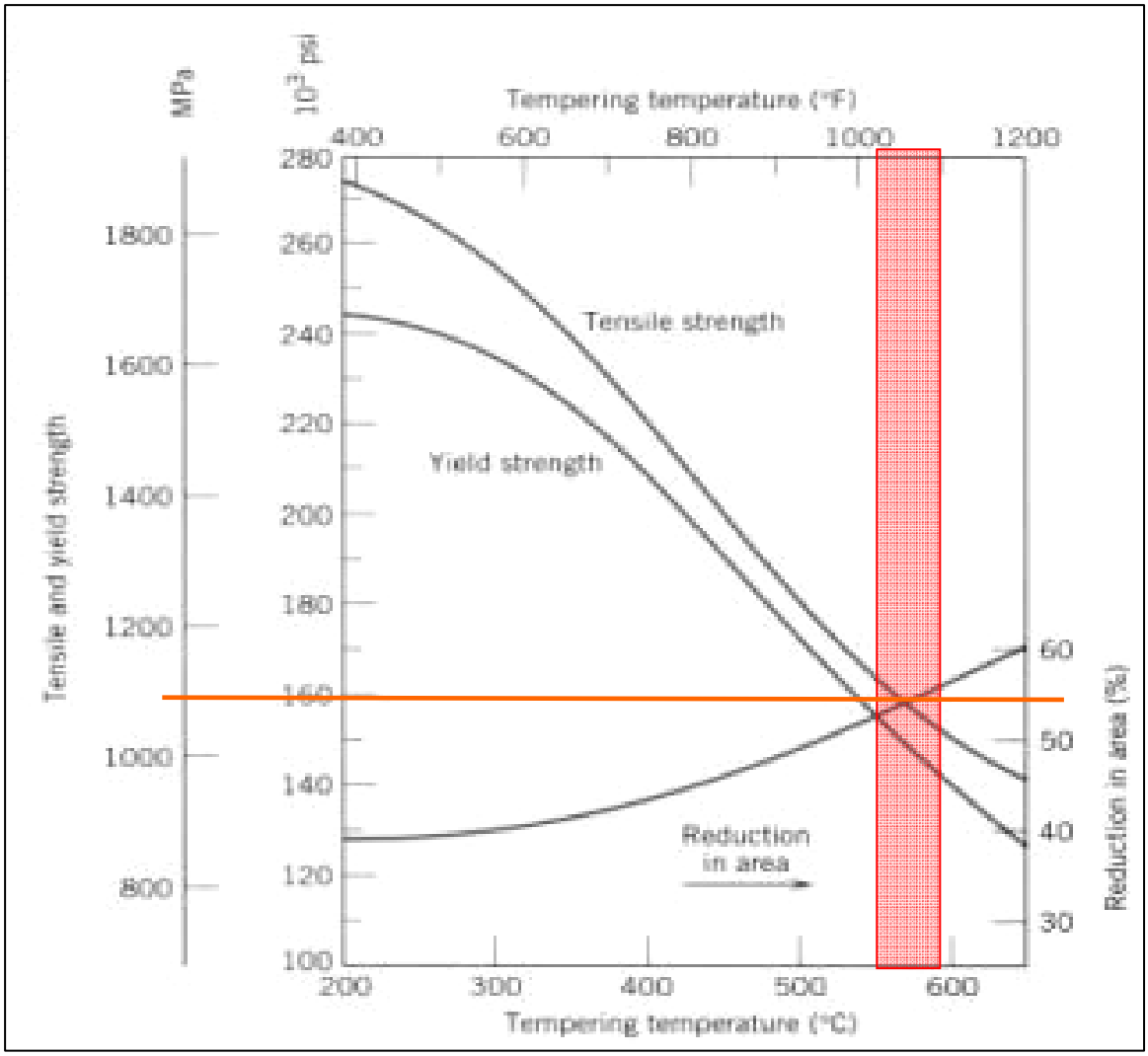

Figure 8. Strength and Ductility vs. Tempering Temperature for 4340 Steel (After Ref. 2)

THIS PAGE INTENTIONALLY LEFT BLANK

III. LABORATORY ANALYSIS

A. INTIAL OBSERVATIONS/VISUAL INSPECTION

The shaft was removed from the spin pit and care was taken to not damage the fracture surfaces on the spindle. Photographs were taken, as shown in Figures 9-13. A cursory visual analysis of the failed shaft and photographs revealed extensive plastic deformation and a generally dull, fibrous surface texture, - two observations that are strongly indicative of ductile failure by microvoid formation and coalescence. Also, the failure plane was approximately 45 degrees to the longitudinal axis, – suggestive of a ductile fracture in tension. The elongation and deformation was most noticeable on the outer diameter of the shaft whereas the inner diameter remained relatively unchanged.

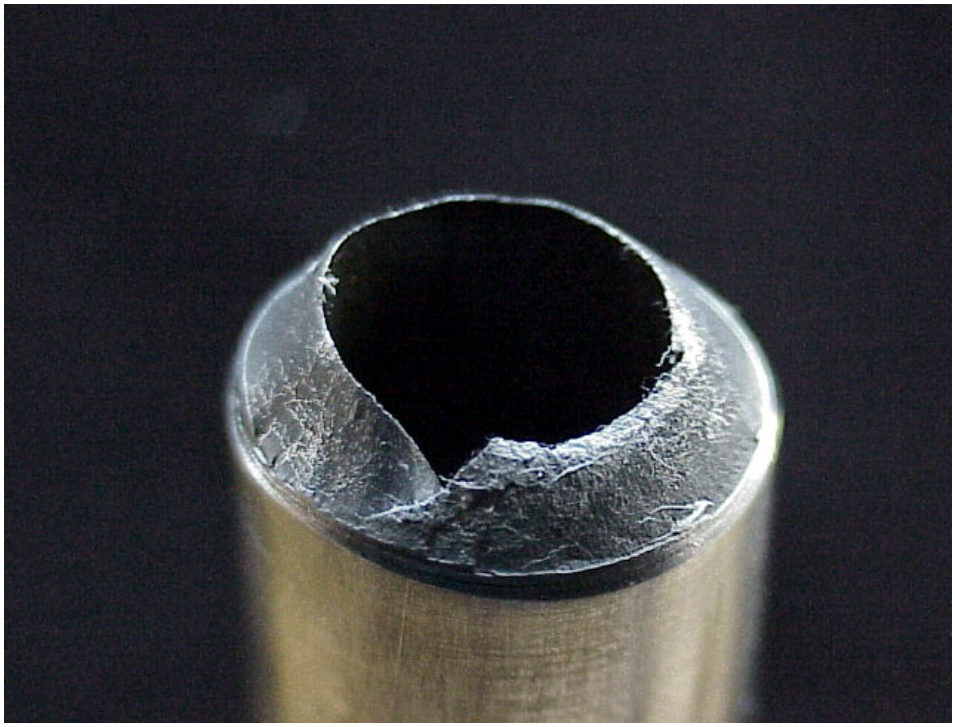

Figure 9. Upper Spindle Fracture Surface

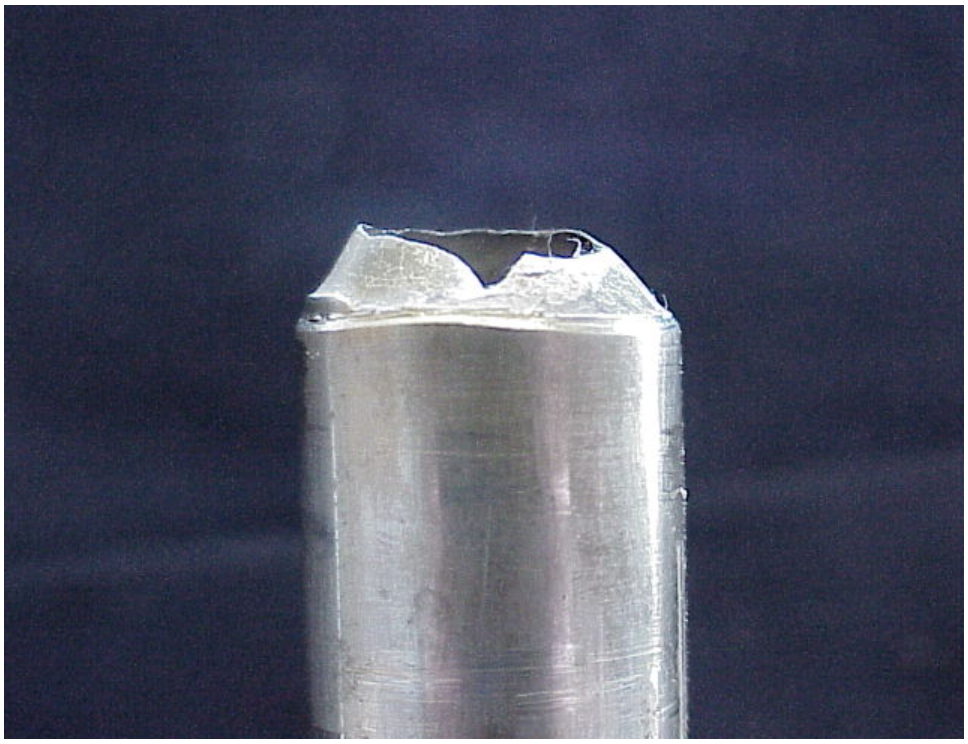

Figure 10. Upper Spindle Fracture Surface (Side View)

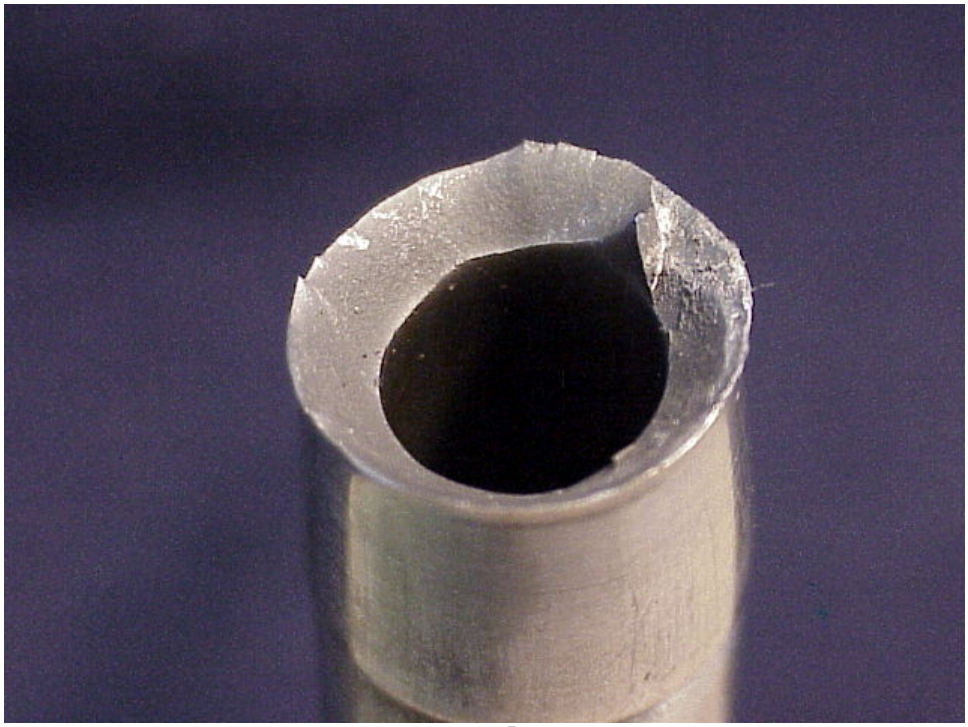

Figure 11. Lower Spindle Fracture Surface

Figure 12. Lower Spindle Fracture Surface (Side View)

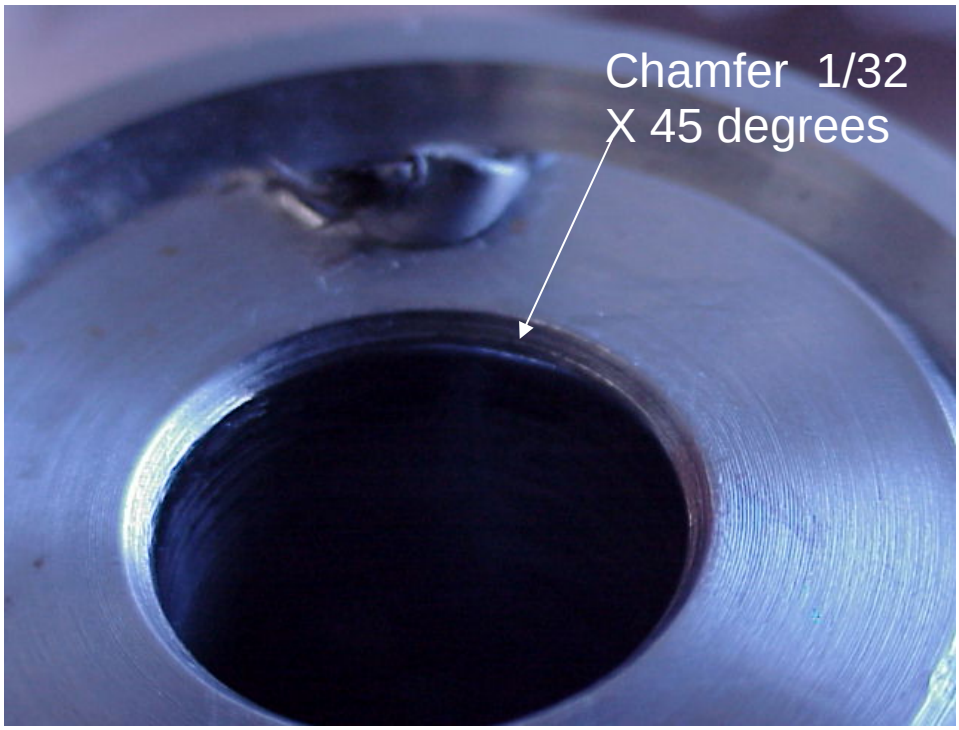

Figure 13. Spindle/Adapter Interface with 45^{o} Chamfer

Figure 13 shows a picture of the adapter/spindle interface, the location where the fracture occurred. One interesting aspect is the 45 degree chamfer at the plane of fracture. This (sharp) chamfer would put a stress raiser on the outer diameter of the shaft. Also, the adapter connected to the spindle shaft through a pinned connection approximately 3 inches below this interface. Because the shaft transmitted torque to the adapter through the double pinned threaded connection, it is possible that a phase shift could have occurred between the shaft and adapter. This shift would have put a torsional stress on the shaft. Both the upper spindle fracture and the adapter interface had a shiny, worn region on the outer and inner diameters, respectively, at the plane of fracture. This shiny, worn region likely would be caused from constant friction and angular movement between the shaft and adapter at the chamfer.

In developing a preliminary failure hypothesis, however, it was thought highly unlikely that tension alone would have caused the failure. The combined stresses from bending, torsion, cyclic (fatigue) and tension were all considered when trying to determine the cause of failure, as well as potential stress raisers in the system.

1. Fatigue Considerations

Given the cyclic loads that were placed on the shaft prior to failure, it was important to consider the possibility of fatigue serving as the dominant failure mode. Fluctuating stresses, or cyclic stress, will result in fatigue failure if the level of stress exceeds the endurance limit of the specimen. With fatigue, the stress can be completely reversible (in which the maximum and

minimum stresses are equal in magnitude but oppositely directed; mean stress is zero) or it can result in a mean stress that is not equal to zero.

Fatigue failure can be classified into two categories: High cycle (HCF) or low cycle (LCF). HCF is characterized by large fatigue regions and small instantaneous regions (representing relatively high fracture toughness). LCF is characterized by small fatigue regions and large instantaneous regions. Due to the magnitude of the stresses involved, LCF failures occur after relatively short lives, whereas HCF has relatively longer lives, when measured in number of cycles.

The three stages of fatigue are: (1) crack initiation, (2) crack propagation (incremental), (3) specimen failure. Crack initiation normally occurs on the surface of the material where a stress concentration has formed. The crack propagates in steps and can have two types of marking called beachmarks and striations. Beachmarks can normally be identified with the unaided eye and symbolize interruptions in applied stress. Striations, which normally must be observed using electron microscopy, represent the distance of advance in a crack front during one cycle. It is important that each of these be identified in the fatigue region of a failed sample, in order to determine if fatigue is a potential mode for failure.

B. PREPARATION

After removing the spindle shaft from the spin pit and performing a thorough visual inspection of the fracture site, the specimen was cross-sectioned twice and the resulting pieces were prepared for further analysis. The

complete lower spindle fracture surface was set aside for Scanning Electron Microscopy (SEM) Analysis. The upper spindle fracture surface was cut into two pieces in the axial direction, mounted, polished and etched with a Nital solution, for examination under the optical microscope. A "donut" cross-section was also taken from the shaft in order to conduct hardness testing of the material. This is shown in Figure 14.

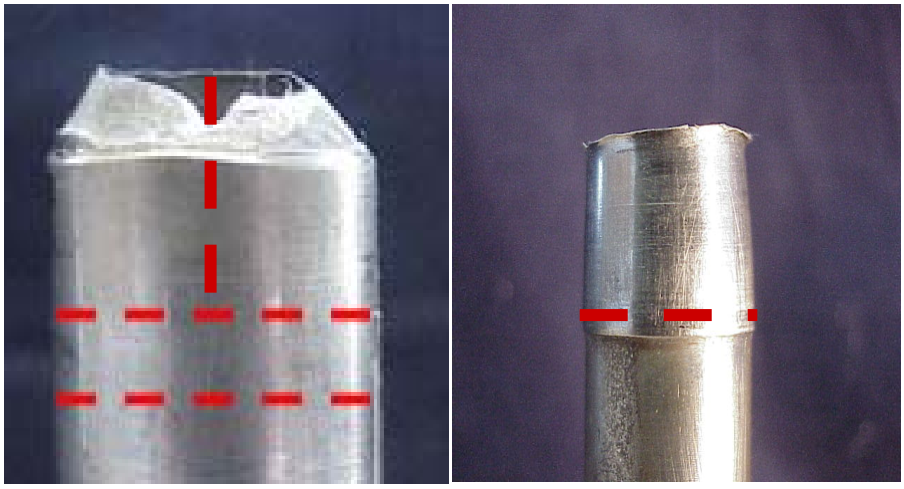

Figure 14. Sectioning of Spindle Shaft

C. HARDNESS TESTING

Hardness testing was performed along the exposed sleeve of the sample using a Wilson MIG1 hardness tester (shown in Figure 15) calibrated for use on the Rockwell C scale. These measurements indicated a material hardness that was consistent with the 32-36 HRC range that was originally specified for the shaft. Six hardness measurements were taken at various places on the "donut" sleeve and a value of 33.5 ± 0.5 HRC was established for the material. As this hardness reading was consistent with the specifications, it helped rule out improper treatment of the material as a possible contribution to the failure of the shaft.

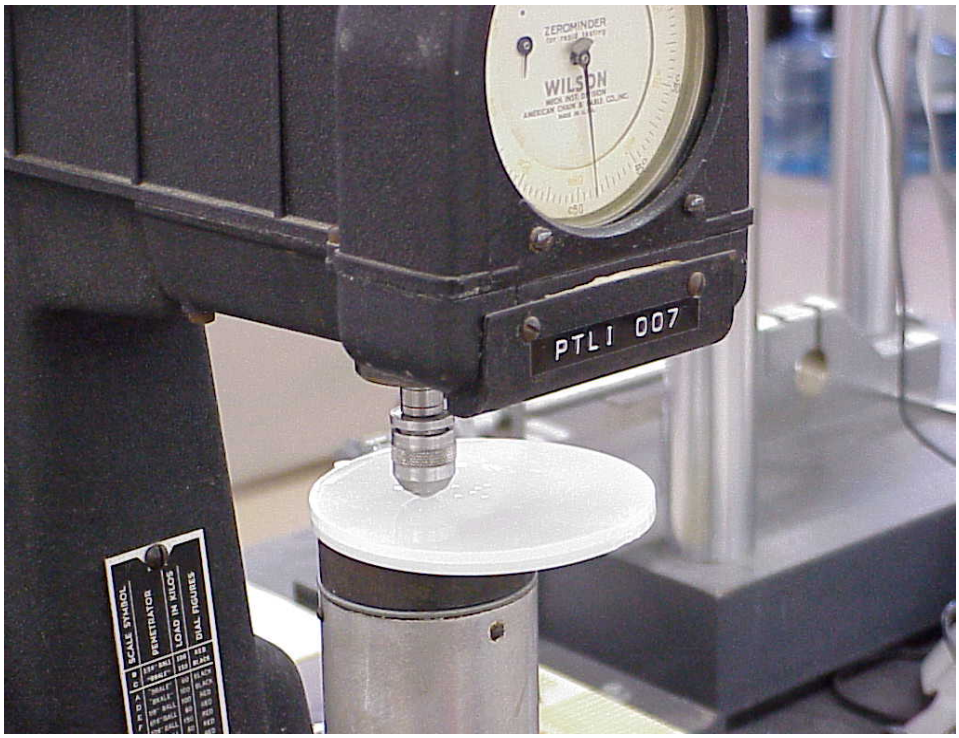

Figure 15. Wilson MIG1 Hardness Tester

D. MICROSCOPIC ANALYSIS

Optical photomicrographs, taken at magnifications of 290×, 750×, and 1500×, provided useful insights into the general microstructure and failure mode of the specimen. Example photographs are shown in Figures 16, 17, 18, and 19, respectively.

1. 290× Magnification

Images taken at 290× magnification (Figures 15 and 16) provided little conclusive evidence as to whether or not the material was potentially flawed. The images taken at this low magnification did provide an exceptional macroscopic image of the fracture surface perimeter and documented the steel’s heat treatment.

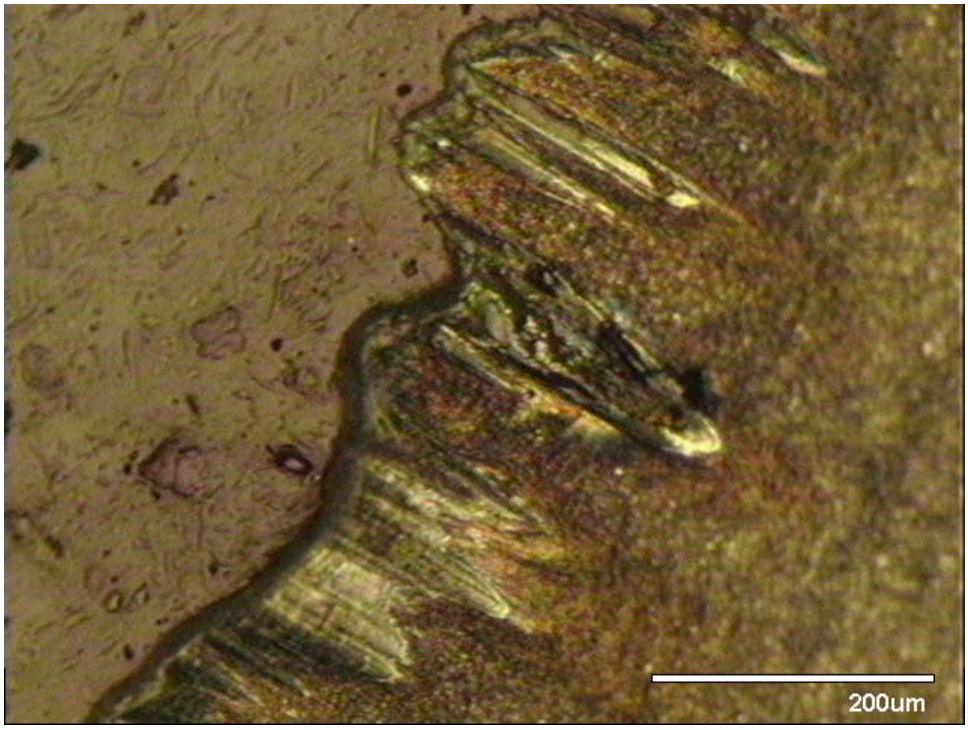

Figure 16. Perimeter of Fracture Region (290×)

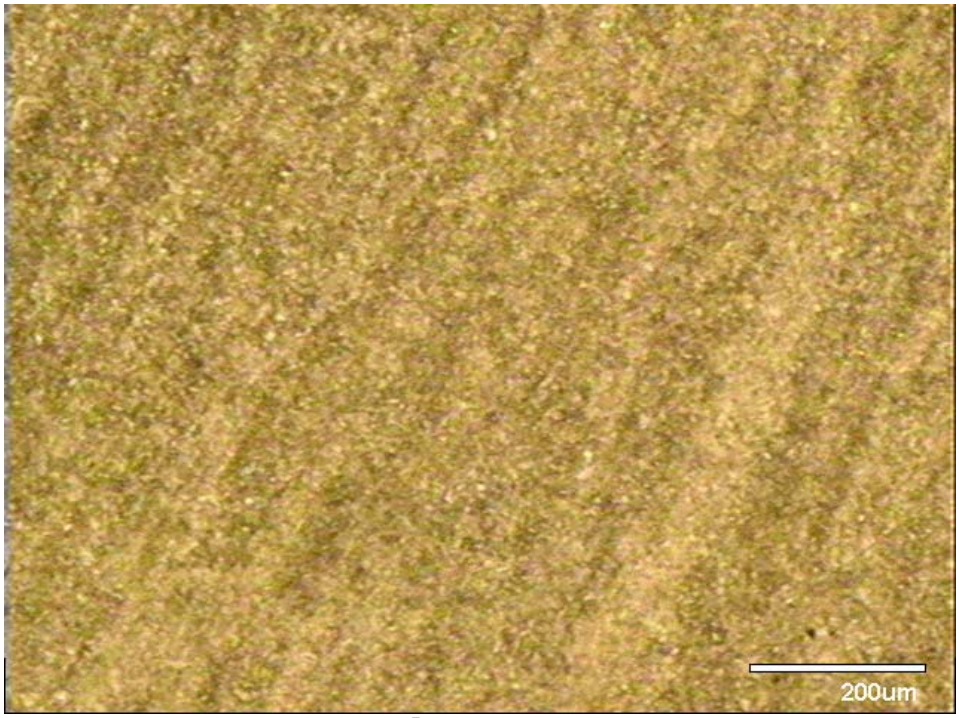

Figure 17. Optical Photomicrograph (290×)

2. 750× Magnification

Under 750× magnification, shown in Figure 18, the microstructure could be confidently identified as tempered martensite. The martensite formed during quenching as carbon was trapped in the lattice as γ austenite transformed to distorted α ferrite. Very fine, needle-like regims of martensite formed with the austenite. Tempered carbides formed as precipitates when the martensite was tempered at elevated temperatures and the carbon was allowed to thermally diffuse out of the martensite's octahedral interstitial sites.

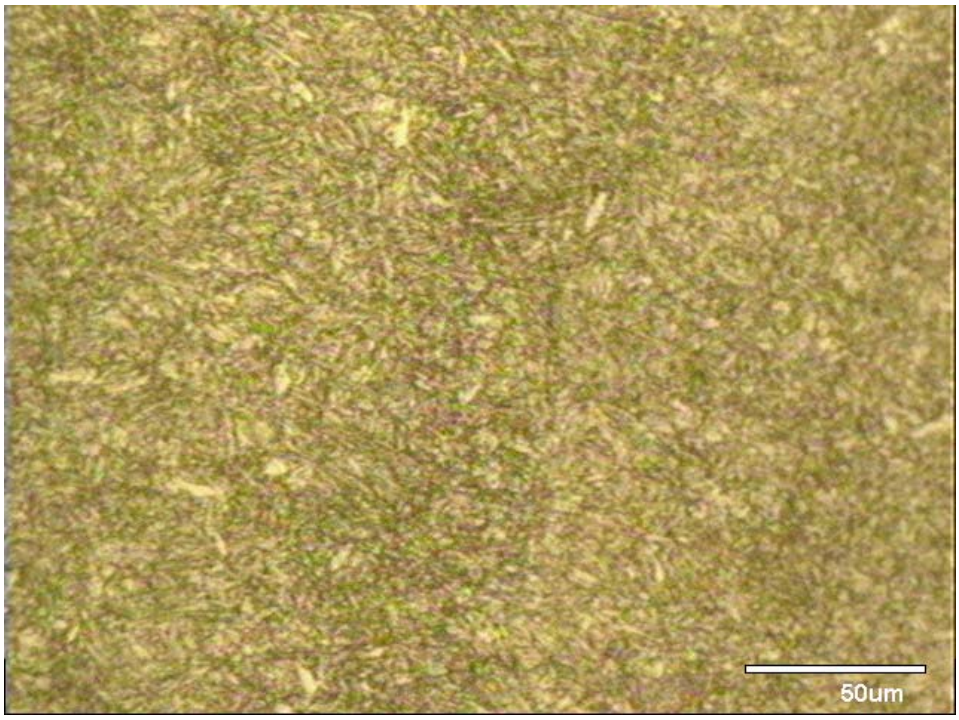

Figure 18. Optical Photomicrograph (750×)

3. 1500× Magnification

At 1500× magnification, shown in Figure 19, the microstructure became still better defined and it was easier to identify the tempered martensite. The cementite particles were very fine. Nevertheless, the needle-like

appearance of the martensite was apparent. This high tempering would result in larger grains, improved ductility and toughness, but substantial loss in strength and hardness.

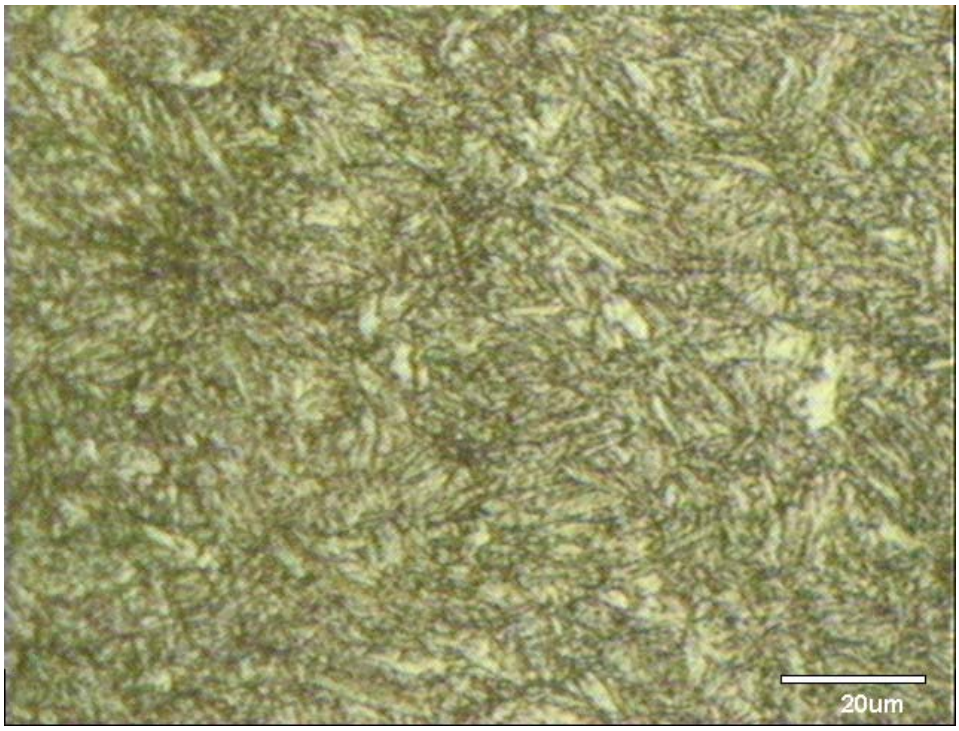

Figure 19. Optical Photomicrograph (1500×)

4. Microscopy Results

Even at high magnification, however, one cannot ascertain whether the steel was completely transformed to 100% martensite using optical methods alone. Alloy steels are popular in industry because the alloy elements (chromium, molybdenum, and nickel) serve to shift the “nose” of the pearlite transformation curve to the right (i.e. larger time scales) of the continuous cooling diagram. This shift relaxes the critical cooling rate (the slowest rate at which austenite can transform to 100% martensite) but does not affect the banite transformation

curve that can be intersected at cooling rates less than 8°C/s from a start temperature of 760 °C.

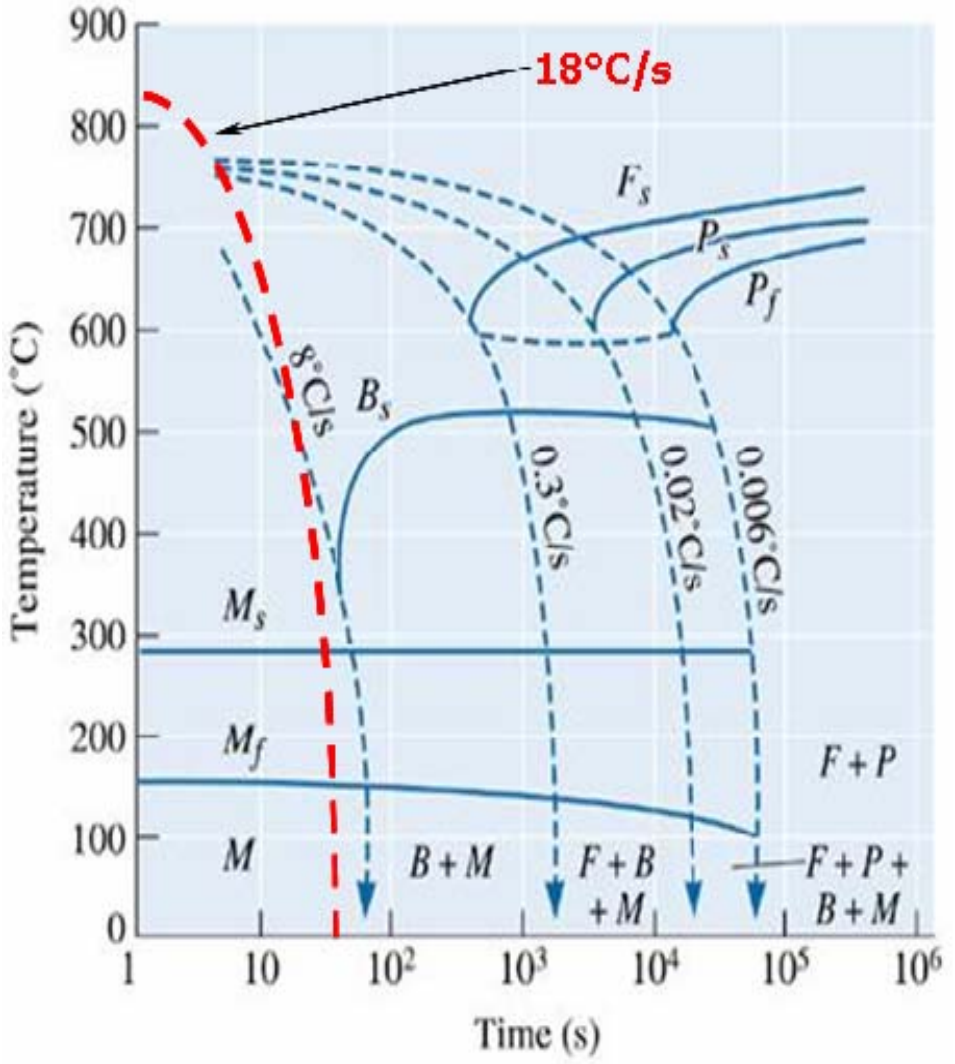

Figure 20. Continuous Cooling Transformation Curve for 4340 Steel (After Ref. 2)

From the continuous cooling transformation curve, shown in Figure 20, and using a conservative cooling rate of 18°C/s for an oil quench hollow shaft, it could be concluded that the spindle microstructure was 100% tempered martensite.

From the optical photomicrographs it was evident that the material microstructure had no definitive flaws and was made within specifications. The failure was in no way due to improper machining or treatment of the steel and was therefore due to excessive stresses in the spindle shaft in its operating environment in the spin pit.

E. SCANNING ELECTRON MICROSCOPY (SEM)

Due to its short effective scanning wavelength and high resolution, SEM analysis proved to be an invaluable tool for evaluating the failure mode. Four SEM photographs were taken of the lower fracture surface.

1. SEM Fractograph #1

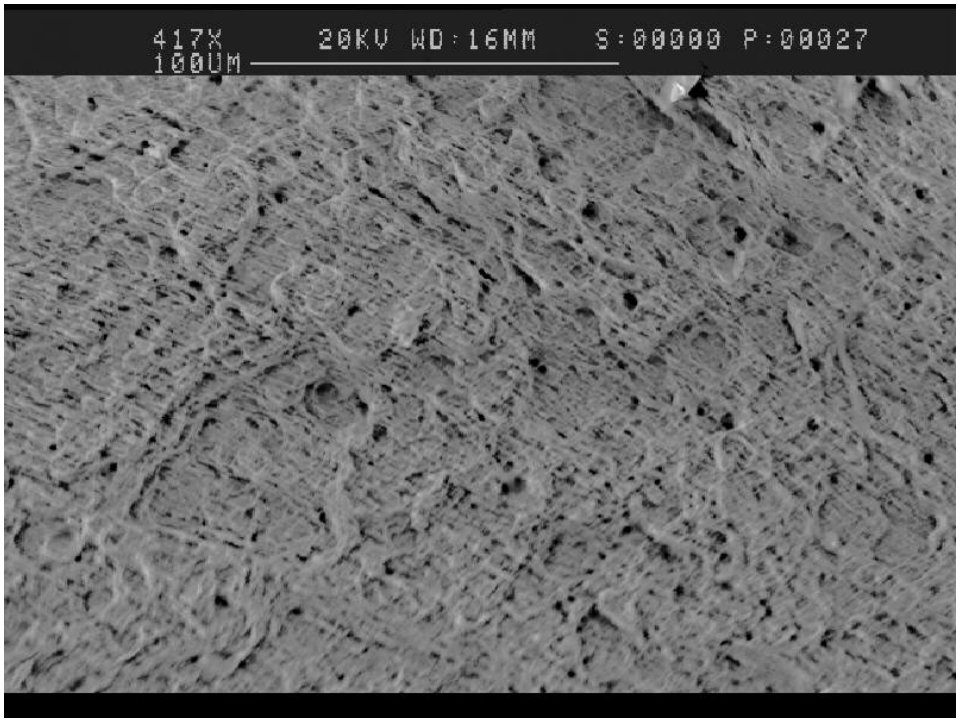

Figure 21. SEM Fractograph 1

Figure 21 shows the first SEM fractograph that was taken near the middle of the failure region. This photo shows a clear case of ductile fracture through microvoid formation and coalescence. The fibrous texture appearance

and microspheres indicate that deformation of the grains and then failure occurred along the grain boundaries. Essentially, the grains were stretched and “plucked” apart leaving spherical voids where the grains from the upper fracture region separated from the lower fracture region.

2. SEM Fractograph #2

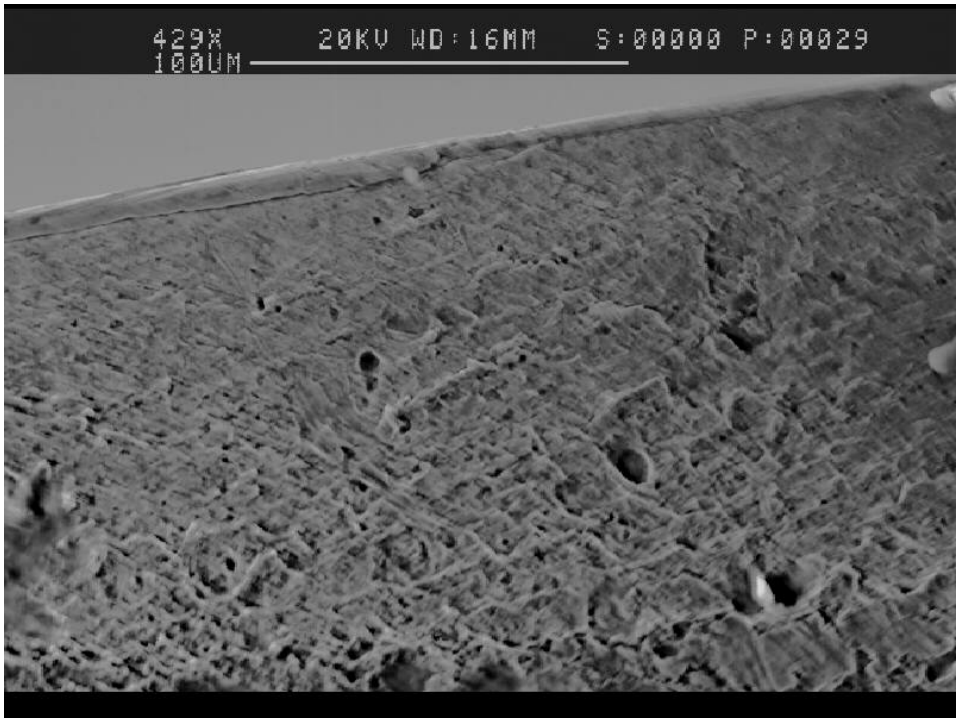

Figure 22. SEM Fractograph 2

Figure 22 shows the second SEM fractograph that was taken towards the outer diameter, on the shear lip, of the spindle shaft failure. In this view, the spherical microvoids begin to become elongated and point towards the origin of the failure. Also, the highly fibrous texture of the surface begins to fade when approaching the outer edge of the shaft. This is due to the transition between the instantaneous and an apparent fatigue zone. Towards the outer diameter a fatigue zone is seemingly present with a

flatter texture and striations are present. These striations are indicative of the cyclic crack propagation.

3. SEM Fractograph #3

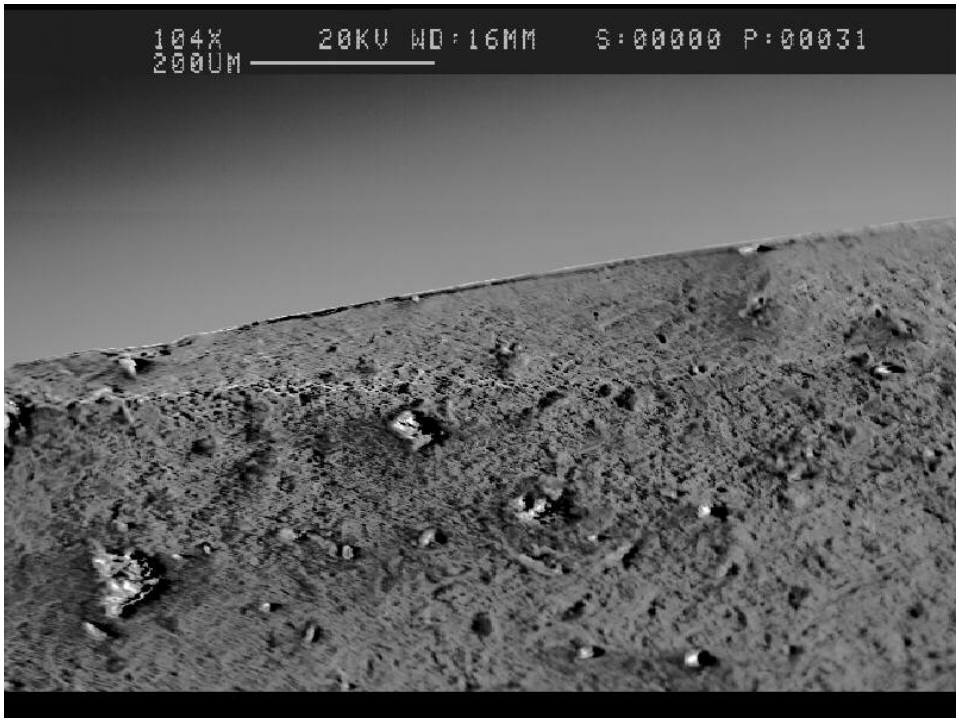

Figure 23. SEM Fractograph 3

Because the elongation of the microvoids pointed towards the outer diameter of the shaft and there was an apparent fatigue zone, another SEM photo was taken around the perimeter. The third photo was taken at a lower magnification in order to see if there was a more pronounced transition between the two zones. Figure 23 shows a different portion of the outer perimeter of the spindle and an even clearer line between the instantaneous zone and fatigue zone. There is a clear difference in surface texture and a solid “ridge-like” line separating the two zones.

4. SEM Fractograph #4 (Crack Initiation)

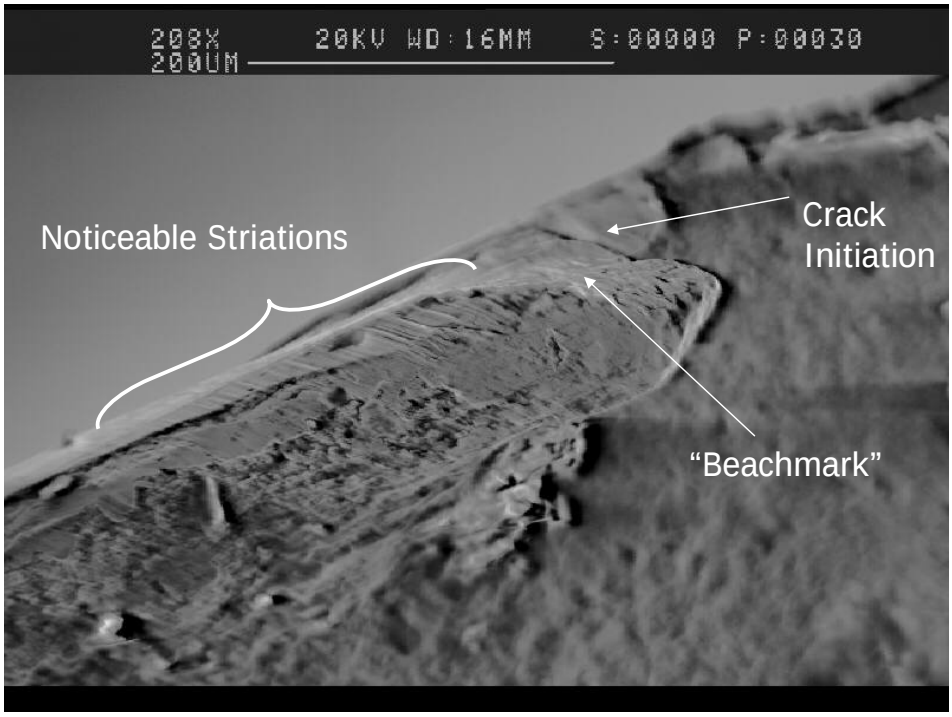

Figure 24. SEM Fractograph 4 (Crack Initiation)

Continuing around the perimeter, an image of the crack initiation point was captured. Figure 24 clearly shows the point of crack initiation. There is a large beachmark present which indicates the large initial propagation of the crack. The noticeable striations indicate the cyclic propagation of the crack that occurred during each spin-up of the spin pit.

5. SEM Results

These four SEM fractographs suggest failure by two distinct modes: (1) low cycle, high-stress fatigue (LCF) and (2) ductile failure through microvoid formation and coalescence. The latter mode is indicated by the presence of numerous spherical, equiaxed microvoids ranging from approximately 1-3 μm, as well as generally fibrous texture of the fracture surface. Fatigue is also strongly

indicated by the presence of striations. Also, the size of the fatigue zone compared to the instantaneous zone is relatively small, less than 10% of entire failure area, which supports the notion of high stress, low cycle fatigue.

F. LABORATORY ANALYSIS SUMMARY

From the visual analysis, Rockwell hardness testing, microscopy and SEM fractographs it can be concluded that the primary cause of failure was a design (or operational procedural) flaw associated with the spin pit system (air turbine, spindle and rotor assembly as a whole) and not the production, processing, or treatment of the material. Micrographs and Rockwell hardness tests both support the conclusion that the 4340 steel used for the spin pit was properly heat treated and did indeed possess the hardness characteristics specified. Furthermore, there were no indications of imperfections within the material or flaws suffered during the processing/treatment of the steel spindle. SEM fractographs provide evidence that high stress, low cycle fatigue was present and that final failure occurred through ductile fracture.

IV. DYNAMIC ANALYSIS

After performing a failure analysis of the spindle shaft it was necessary to obtain the mode shapes present and the associated natural frequencies. The mode shapes and natural frequencies are critical when operating the spin pit because any operation near these frequencies can cause destructive resonance and eventually failure. Unfortunately, the natural frequencies had never been determined and were only approximated.

A. ADVANCED ROTATING MACHINERY DYNAMICS PROGRAM

In order to accomplish the modeling of the system, a dynamic modeling software package from Rotor Bearing Technology & Software (RBTS) was used. The Advanced Rotating Machinery Dynamics (ARMD) software package is capable of performing analysis of lateral vibration (rotor dynamics), torsional vibration, fluid-film bearings, rolling element bearings and a lubricant analysis. In order to determine the mode shapes and their associated natural frequencies, the lateral and torsional vibration programs were used.

1. Theory

In order to determine the mode shapes and natural frequencies the system is broken into a system of components each with differential equations based on a rigid rotor with one degree of freedom and free vibration. The following is the dynamic equation and the characteristic solution used to solve for the mode shapes and frequencies (From Ref. 4):

$$MX'' + DX' + KX = 0 \qquad (1)$$

$$X_c = X_o e^{\alpha t} \qquad (2)$$

$$\lambda = \alpha + i\omega \quad (3)$$

Solution:

$$X_c = X_o e^{\alpha t}(\cos \omega t + i \sin \omega t) \quad (4)$$

X_o = Mode Shape

ω = Frequency

2. Modeling

In order to begin modeling the system, the turbine assembly (Figure 2) and the adapter, collar and arbor assembly (Figure 4) were studied. Due to the program's inability to model a shaft within a shaft, the system had to be modeled in two branches. The first branch included the turbine wheel and the second branch included the speed nut, spindle shaft, adapter, collar, arbor and rotor. Figures 25 and 26 show the ARMD model for the two branches constructed. The two branches are connected at the threaded connection between the speed nut and the turbine shaft. In order to account for the turbine shaft branch in the spindle shaft branch, a fictional spring was added at the point of connection. An external force was then applied to the turbine shaft branch in order to measure the displacement of the connecting node. Finally the fictional spring constant was determined by dividing the external force by the connecting node displacement.

Figure 27 shows the torsional model that was used in order to determine the natural torsional modes that were present. The torsional program in the ARMD software package allowed for the connection of the two branches from the rotor dynamics analysis. The models that were

initially constructed in the rotor dynamics sub-program (Figures 25 and 26) were imported and connected at the node of connection, the rotor speed nut/turbine wheel shaft threaded connection.

For more information on the ARMD software package or modeling refer to Appendix A, the “ARMD V5.0G1 User’s Manual (Ref. 3),” or the “Bearing & Rotor Dynamics Seminar: Fluid-film/Rolling Element Bearing Technologies and Rotordynamic Interactions-Lecture Notes (Ref. 4).”

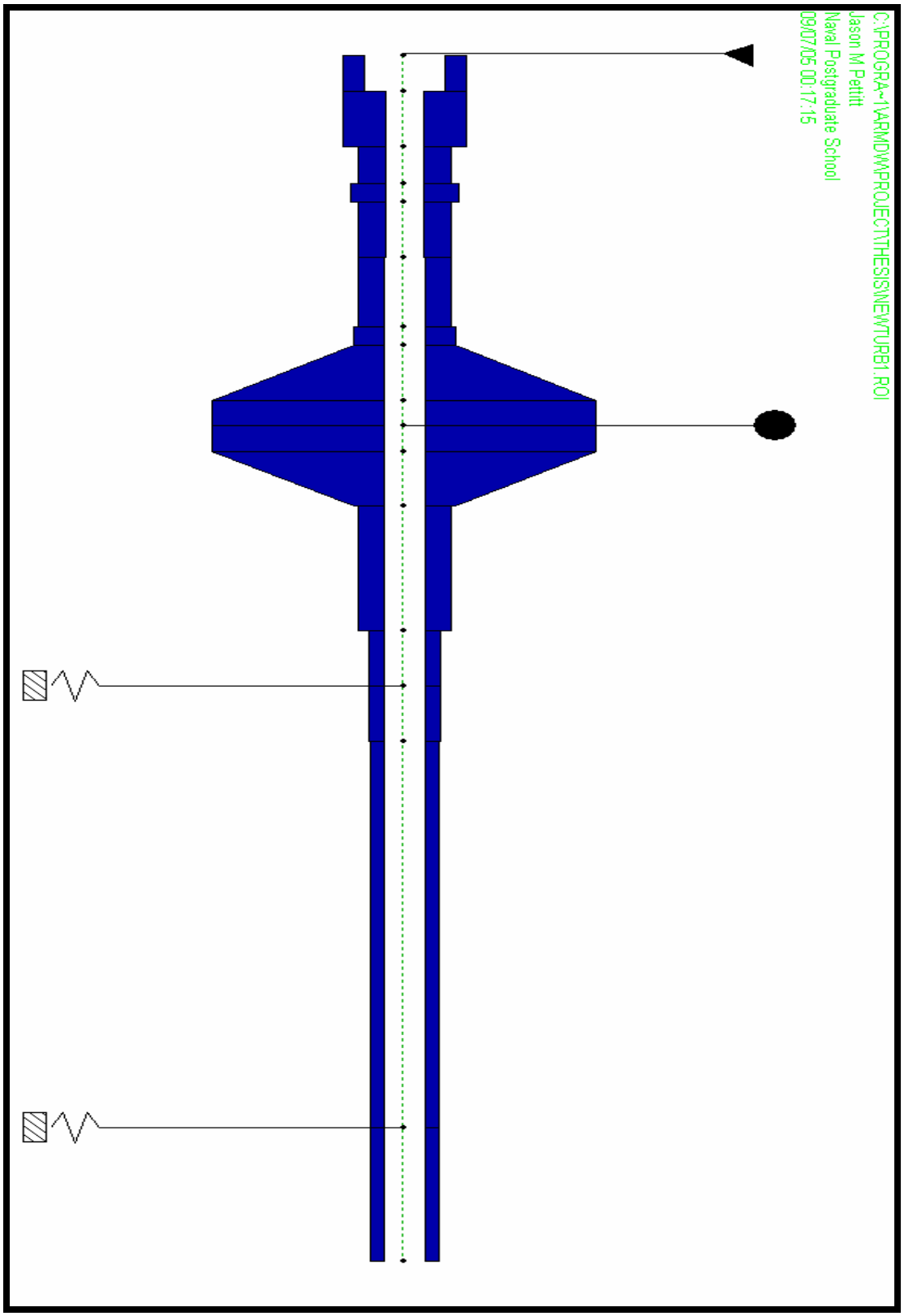

Figure 25. Turbine Wheel Branch Model

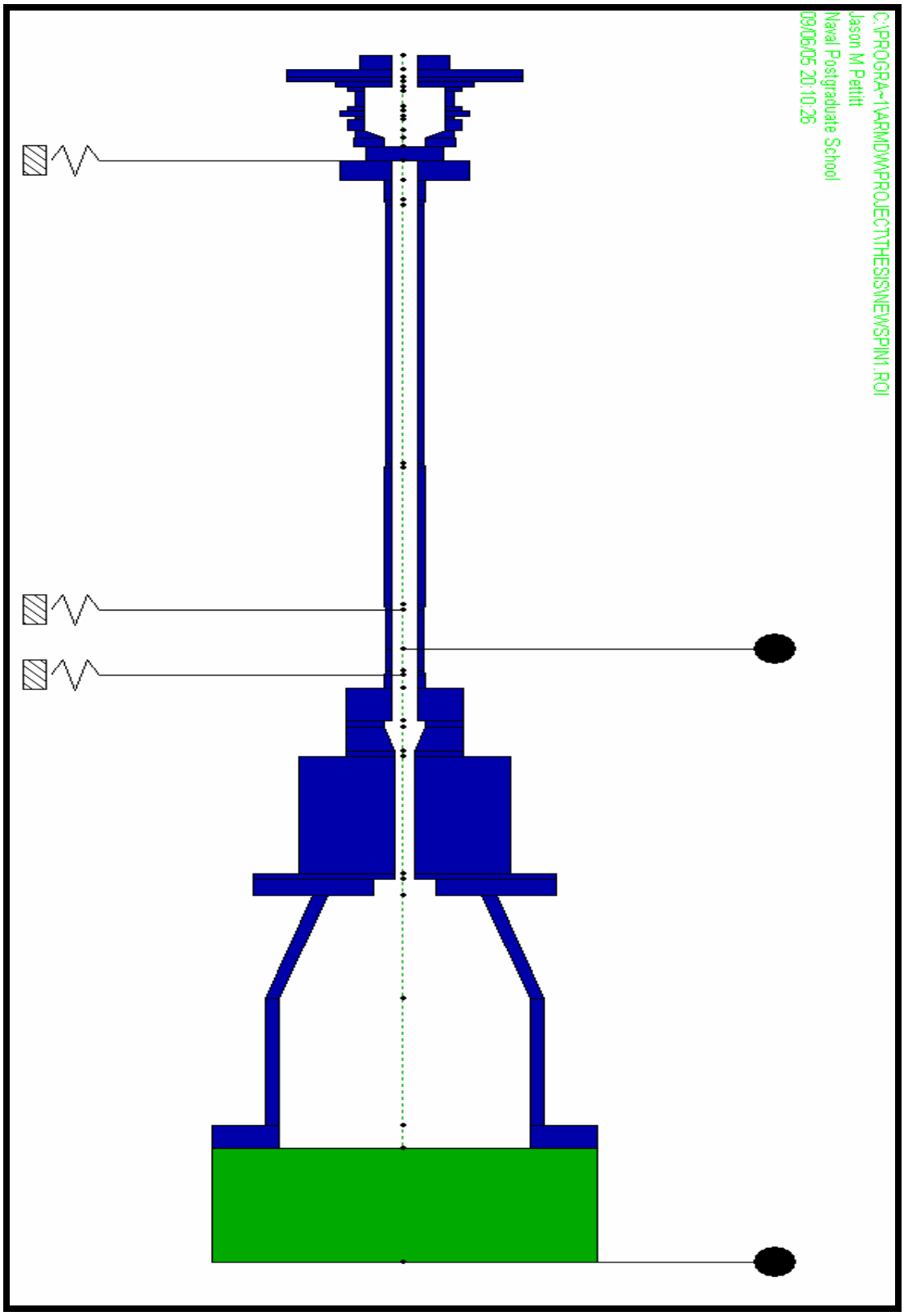

Figure 26. Spindle Shaft Branch Model

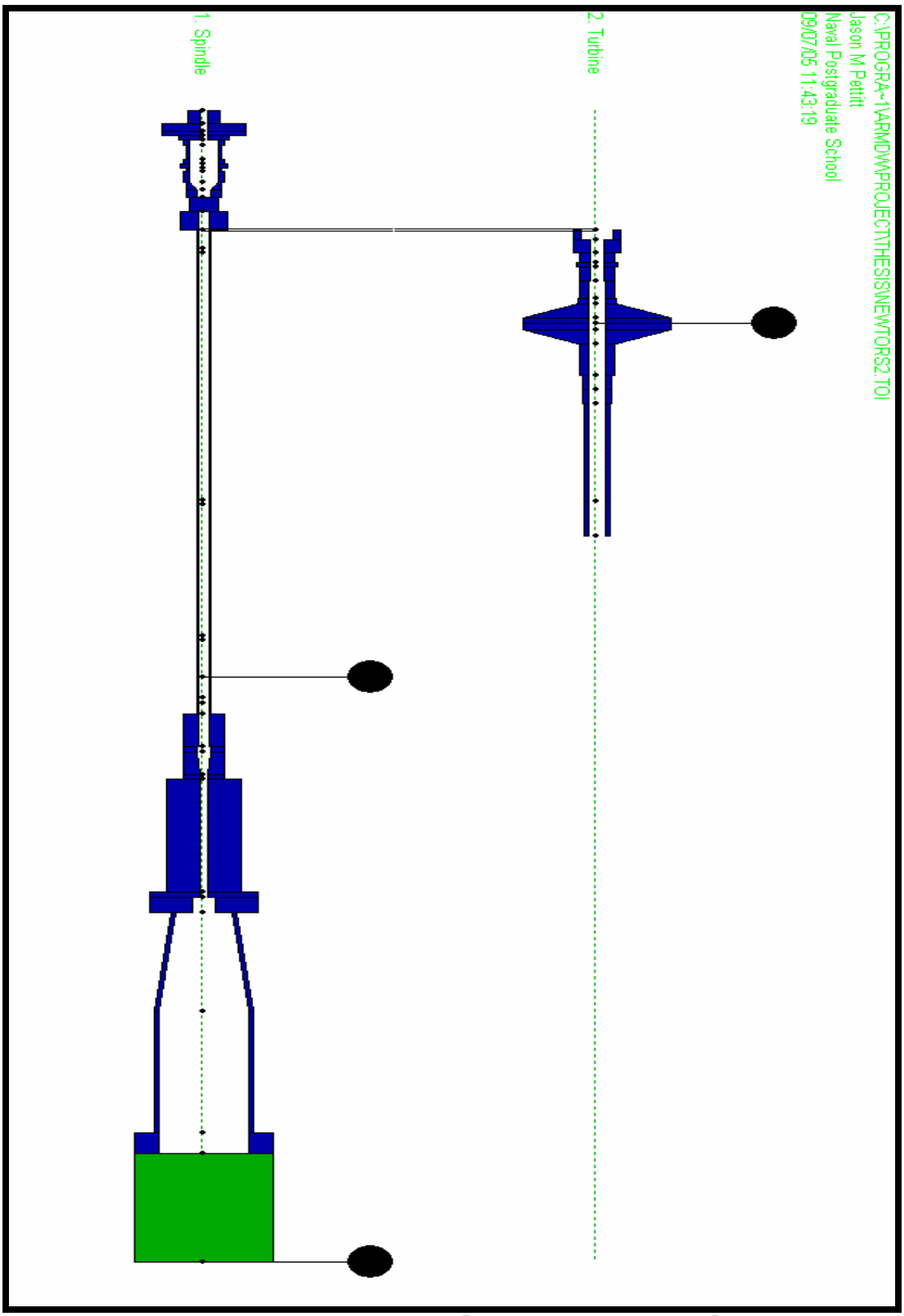

Figure 27. Torsional Vibration Model

B. ANALYSIS AND RESULTS

After completing the model, the stability analysis program was run in the Rotor Dynamics portion of the ARMD software package. The results yielded the modes and natural frequencies present. The results are given in a Campbell Diagram in Figure 28.

The Campbell Diagram shows the bending and torsional modes that are present and the natural frequencies at which they exist. Because the spin pit is an overhung rotor, gyroscopic effects affect the modes present. There is a pendulum mode present and at rest it occurs at approximately 200 RPM. However, as the system increases it speeds, the pendulum mode will divert into a forward and reverse precessional.

From the Campbell diagram it is clear that the only bending mode that could possibly present a problem is the 1^{st} bending mode. However, this mode intersects the operating line (1/rev) at approximately 4300 RPM, which is outside the normal operating speed range. As long as the speed of the system never dwelled at this speed, no damage would have occurred due to 1^{st} bending.

The torsional vibration analysis yielded two torsional modes that existed within the operating speeds. The first torsional mode is present at an insignificantly low speed of approximately 15 RPM. However, the second torsional mode is located at approximately 2350 RPM. This mode is close to the speed of 2500 RPM where failure occurred.

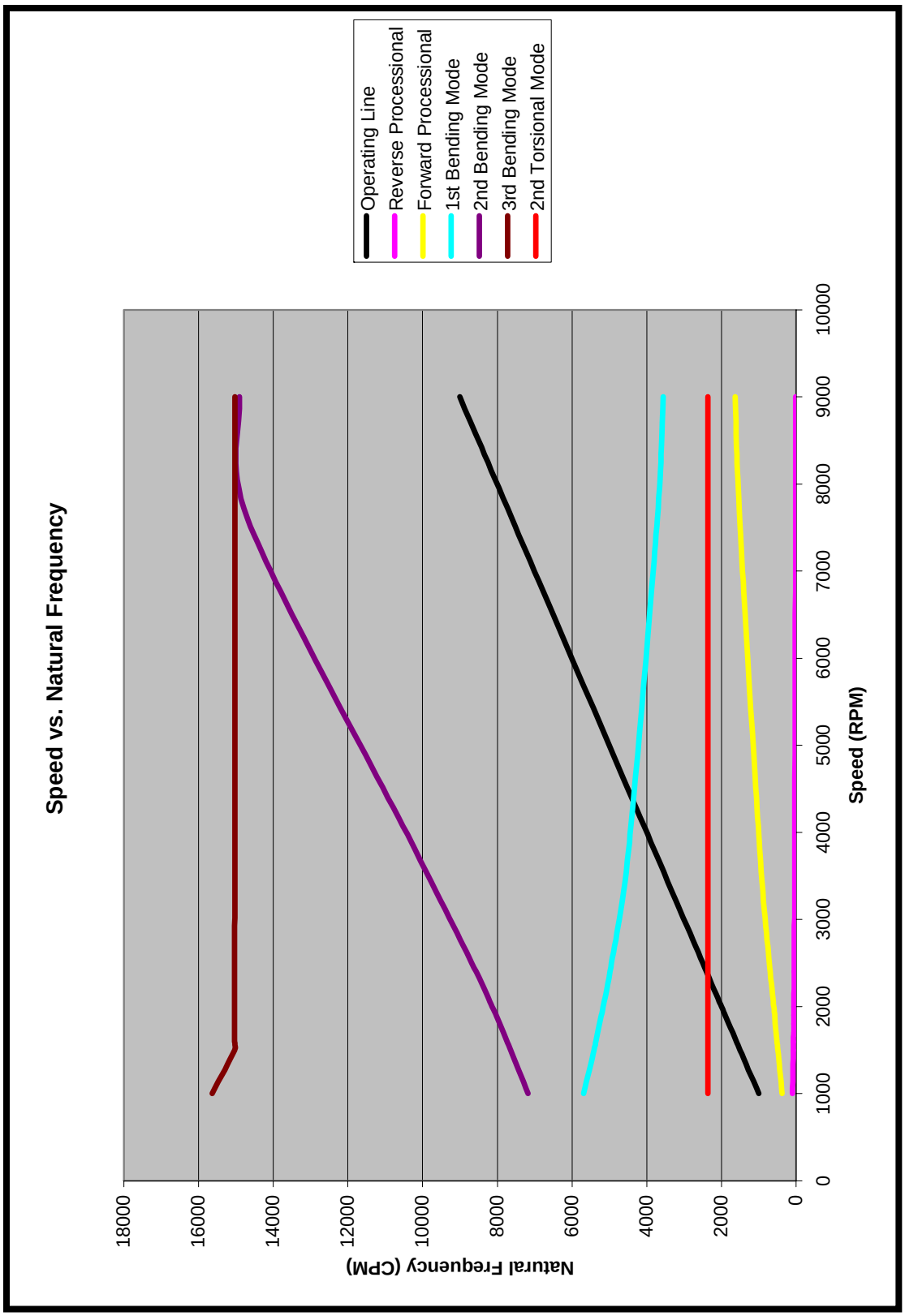

Figure 28. Campbell Diagram

V. CONCLUSIONS

A. PUTTING THE PIECES TOGETHER

From the material failure analysis and the dynamic modeling of the system it is clear that the material failure occurred due to a system design flaw, or perhaps more accurately, the failure to change spindle shafts well within the LCF lifetime. The 4340 steel with which the spindle shaft was formed was within specifications and there was no indication of imbedded flaws. The material's hardness and microstructure were wholly consistent with specifications.

The evidence surrounding this fracture event strongly supports the conclusion that two modes of failure (high stress, low cycle fatigue, followed by ductile fracture) were responsible for system failure. Failure most likely resulted from fatigue-generated crack initiation at the external surface, followed by incremental crack propagation and finally, upon reaching critical crack length-instantaneous ductile failure by microvoid formation and coalescence.

B. TIMELINE OF EVENTS

The following is a suggested timeline of events from the start of use of the spindle shaft until its failure.

The spindle shaft was made from 4340 steel that was austenitized, oil quenched, and tempered. The shaft was then fitted for use with the 8-inch Barbour-Stockwell air driven turbine and used in the Rotor Spin Research Facility. The shaft was in use for several years and used with numerous rotor test articles. Sometime during normal operation, the spindle shaft was damaged from either

bending and/or torsion. The shaft continued to be utilized in the spin pit and fatigue crack propagation occurred. Because the apparent fatigue is high stress, low cycle fatigue, the crack likely occurred during testing with one of the AE3007 Rotors attached (either configuration 1 or 2).

There are several factors that could have contributed to the damaging of the spindle shaft during normal operation. The residual imbalance of the entire spin assembly could essentially change and excite the present modes. Also, if the test rotor was not properly balanced (during the last build) the same is likely. Also, at the adapter/spindle interface, the 45 degree chamfer will raise the stresses on the outer diameter of the spindle. Finally, the potential phase shift between the spindle shaft and adapter due to the pinned connection would increase the torsional stresses within the spindle.

On 14 March 2005, the system was operated and spun up to 1000 RPM, then drifted slowly to 1600 RPM and finally increased to 2000 RPM. Upon increasing the speed to a desired target speed of 7600 RPM, the shaft failed at approximately 2500 RPM. Because the shaft already had extensive damage from the initial crack and subsequent fatigue propagation, when the system ran through the 2^{nd} torsional mode (~2350 RPM) it became excited and resonant, even if only briefly. This excited state caused significant crack propagation and induced ductile failure after a critical crack length was reached for the given tensile load.

C. RECOMMENDATIONS

In the interest of preventing this type of failure in future tests, some recommendations for changes to the system and its operation are made. First, although the standard 1000 RPM dwell speed is away from bending and torsional modes, the ARMD program does not have the ability to couple bending and torsion together in a single analysis. Therefore, because the most harmful resonant modes are at lower operating speeds, it is recommended that all system checks be performed before start up, or expedited as much as possible, and speed quickly increased to the target operating speed. Also, an increase in thickness of the spindle shaft is recommended. An increase in thickness will decrease the stresses on the outer diameter of the shaft. Also, by increasing the thickness, critical crack depth will increase and crack presence should be easier to identify. With this increase, it is also recommended that a visual inspection of the system be performed after every test. Special attention should be given to the spindle shaft, thoroughly looking for cracks and deformation. At the spindle/adapter interface, it is recommended that the 45 degree chamfer be changed to a radiused chamfer in order to alleviate the stresses at the plane where the fracture took place. Also, proximity probes should be placed above the interface (on the spindle shaft) and below the interface (on the adapter). Two probes should be placed at each location and should be set 90 degrees apart. They should then be monitored in order to determine if there is a substantial phase shift occurring between the spindle and adapter configuration. Finally, it is recommended that staff at the Turbopropulsion Laboratory take a training course or

seminar from Rotor Bearing Technology and Software (RBTS) in order to make the most of the capabilities of the ARMD Software Package in future programs. Continuation of modeling is essential and can only improve with added time and understanding.

APPENDIX A – ARMD SOFTWARE TUTORIAL

1. Install ARMD Software Package and Dongle Device Driver.
2. Open ARMD Program
3. Click on “Rotor Dynamics” Sub-program
4. Read and Complete ROTLAT Tutorial
5. Click “Project” Tab and Select “New”
    a. Enter Name of Project
6. Click “File” Tab and Select “New”
    a. Select Unit of Measurement
7. Click “System” Tab
    a. Select “Materials”
        i. Enter the properties of the different materials present in the system to be modeled (i.e. Modulus’ of elasticity, density)
    b. Select “Elements”
        i. Divide the system into elements with appropriate boundaries/nodes present
            1. Under the TP (type) column, enter the appropriate shaft type
                a. Right click to see options
            2. Under the MT (material) column, enter the corresponding material number for that particular element

3. Under Length, enter corresponding element length
4. Under OD1, enter corresponding element outer diameter at left hand node boundary
5. Under ID1, enter corresponding element inner diameter at left hand node boundary
6. Under OD2, enter corresponding element outer diameter at right hand node boundary
7. Under ID2, enter corresponding element inner diameter at right hand node boundary

c. Select “Discs”

i. Enter any discs that are present in the system

1. Under Node, enter the appropriate node where the disc is located
2. Under Weight, enter the weight of disc
3. Under WR^2, enter the disc’s polar moment of inertia
4. Under Transverse, enter the disc’s transverse moment of inertia
5. Under Unbalance, enter the disc’s residual unbalance (found in Section 3 of Ref. 4, U=4W/N)

6. Under Name, enter appropriate label to differentiate discs (i.e. rotor)

d. Select “Bearings”

i. Enter any bearings that are present in the system

1. Under Node, enter the appropriate node where the bearing is located

2. Under DOF, keep the degrees of freedom equal to 2

3. Under Type, enter appropriate bearing type

a. Right click to see options

e. Select “Speeds”

i. Enter speeds that need to be analyzed

1. Right click to enter bearing coefficients

a. For bearing stiffness, k, the stiffness should be duplicated along the diagonal ([1,1] and [2,2])

8. Click “Options” Tab

a. Select “Problem Description”

i. Enter description, this will be displayed upon system model

b. Select “Output Control”

i. Enter the number of modes wished to be determined for the system (i.e. 10)

ii. Enter any gravitational body forces in either the X- or Y- direction

c. Select “External Forces”

i. Enter any external forces that are applied to the system

1. Under Node, enter the appropriate node where the external force is located

2. Under Direction, enter the appropriate direction of the external force

a. Right click for options

3. Under Magnitude, enter the appropriate magnitude of the external force

9. Click “Run” Tab

a. Select “Stability Analysis”

i. Select speed at which to run the analysis

1. Click “View” Tab

a. Select “System Model”

i. To see mode shapes hold “Shift” and tap “Page Dn” buttons

ii. To see mode animation hit “F7” then tap the “+” or “-“ buttons to speed or slow the animation

b. Select “Text Output”

i. The text output will give nodal calculations and displacements

b. Select “Unbalance Response”

i. Select initial, intermediate and final speed

1. The option to view text output is given

10. Click “View” Tab

a. Select Graphics Output

i. Choose either “Stability Analysis” or “Unbalance Response”

1. Graph Options will display

a. Click “Plot 1” and select the X- and Y- axis data to be plotted

THIS PAGE INTENTIONALLY LEFT BLANK

LIST OF REFERENCES

1. Askeland & Phule, Science & Engineering of Materials, 4th Ed., Thompson Press, December 2002.

2. Callister Jr., William D, Materials Science & Engineering, 6th Ed., John Wiley and Sons, July 2002.

3. "ARMD V5.0G1 User's Manual," Rotor Bearing Technology & Software.

4. "Bearing & Rotor Dynamics Seminar: Fluid-film/Rolling Element Bearing Technologies and Rotordynamic Interactions-Lecture Notes," Rotor Bearing Technology & Software.

THIS PAGE INTENTIONALLY LEFT BLANK

INITIAL DISTRIBUTION LIST

1. Defense Technical Information Center
   Ft. Belvoir, VA

2. Dudley Knox Library
   Naval Postgraduate School
   Monterey, CA

3. Department Chairman, Code ME/Hy
   Department of Mechanical Engineering
   Naval Postgraduate School
   Monterey, CA

4. Professor Emeritus Raymond P. Shreeve, Code ME/Sf
   Department of Mechanical Engineering
   Naval Postgraduate School
   Monterey, CA

5. Curriculum Officer, Code 570
   Department of Mechanical Engineering
   Naval Postgraduate School
   Monterey, CA

6. Professor Terry R. McNelley, Code ME/Mc
   Department of Mechanical Engineering
   Naval Postgraduate School
   Monterey, CA

7. Raymond Pickering
   Propulsion and Power Engineering
   Naval Air Systems Command (AIR4.4)
   Patuxent River, MD

8. Frank Lieghley
   USAF AFRL/PRTS
   Wright-Patterson AFB, OH

9. ENS Jason M. Pettitt
   United States Navy
   Norfolk, VA